SPATIAL & TEMPORAL CONTROLS ON THE INORGANIC CARBON SYSTEM OF THE WESTERN ARCTIC OCEAN

by

Andrew Collins

A thesis submitted to the Faculty of the University of Delaware in partial fulfillment of the requirements for the degree of Master of Science in Marine Studies

Summer 2016

SPATIAL & TEMPORAL CONTROLS ON

THE INORGANIC CARBON SYSTEM

OF THE WESTERN ARCTIC OCEAN

by

Andrew Collins

Approved: _____

Wei-Jun Cai, Ph.D.
Professor in charge of thesis on behalf of the Advisory Committee

Approved: _____

Mark Moline, Ph.D.
Director of the School of Marine Science & Policy

Approved: _____

Mohsen Badiey, Ph.D.
Acting Dean of the College of Earth, Ocean and Environment

Approved: _____

Ann L. Ardis, Ph.D.
Senior Vice Provost for Graduate and Professional Education

ACKNOWLEDGMENTS

I'd like to acknowledge the following people for their help and support during my pursuit of this degree: Drs. Wei-Jun Cai, Mark Moline, Mark Warner, Baoshan Chen, Victoire Rerolle, Matthew van der Humphreys and Shigeto Nishino. Also thanks to Qi Di, Veronique Oldham, Scott and Rosette Collins, and my fellow students and friends. Special thanks to the National Science Foundation for funding this research.

TABLE OF CONTENTS

LIST OF TABLES

LIST OF FIGURES

ABSTRACT

The Arctic Ocean plays a critical role in the global carbon cycle. It is believed to be particularly sensitive to the effects of climate change, is already undergoing dramatic changes, and is therefore important to study in that context. Most studies of the inorganic carbon system in the Western Arctic focus on hydrographic datasets from summer and/or fall (July-October), and do not consider the full response of the system to the timing of ice retreat, organic matter production and remineralization, and ice advance. Here we present the first dataset to investigate the spatial and temporal controls on the inorganic carbon system from early spring (pre-phytoplankton), late spring (initial phytoplankton bloom), summer (post-bloom), and fall in 2014. Our results suggest that the timing of ice retreat has important implications for the length of the phytoplankton growing season, and thus influences the magnitude of biological carbon cycling. We extend our analysis to include high-resolution temporal estimates of air-sea CO_2 flux, and estimate a total annual CO_2 uptake in the Chukchi Sea of ~7.7 Tg C. This is the first dataset to evaluate the importance of different seasonal observations within one year on the annual uptake of CO_2 in the western Arctic Ocean. Our results show that extrapolations from one observational dataset result in large over- or underestimations of annual CO_2 flux.

Chapter 1:

INTRODUCTION

The Arctic Ocean, which occupies only ~3% of the global ocean surface and ~1% of its volume, plays an important role in global ocean processes such as intermediate and deep water formation (Aargaard et al., 1985; Tanhua et al., 2009), and atmospheric CO_2 uptake (e.g. Semiletov et al., 2004; Bates, 2006; Evans et al., 2015). Recently, the Arctic Ocean has experienced dramatic and widespread changes owing to global climate change (Overpeck et al., 2005). Atmospheric warming in the Arctic has occurred at approximately twice the rate of the global average, resulting in a precipitous decline in the thickness and extent of sea-ice in the past several decades, with 2012 exhibiting the lowest sea-ice volume on record (Serreze et al., 2003; Stroeve et al., 2007; Jeffries et al., 2014). Decreased albedo in ice-free areas promotes increased solar absorption, driving further melting and reduced wintertime ice formation (Perovich et al., 2007; Schroder et al., 2014). A transition from thick, multi-year ice to fragmented, mobile first-year ice has allowed for enhanced wind-driven circulation and mixing in the surface ocean (Carmack & Chapman, 2003; Yang, 2009). Furthermore, changes to the freshwater content in the Arctic ocean due to enhanced sea-ice melt and river discharge (Peterson et al., 2002; Yamamoto-Kawai et al., 2009; Giles et al., 2012) affect surface ocean stability, which in turn affects biological productivity and ocean circulation (Nishino et al., 2011). Circulation changes, such as increased inflow of warm Pacific water (Woodgate et al., 2012) and decreased transport of the Alaskan Coastal Current (Brugler et al., 2014) are changing

nutrient inputs, upper halocline ventilation, and seasonal ice cover in the central basin.

All of these changes have important implications for the future of the Arctic Ocean carbon cycle. Several authors (e.g. Bates, 2006; Lepore et al., 2007) have discussed the importance of the continental shelf pump as the main mechanism of inorganic carbon storage in the Arctic, whereby carbon fixed into organic matter (OM) is remineralized following the phytoplankton growing season and is supplied to and thus stored in the Canada Basin. Recent changes in the timing and magnitude of biological productivity have been linked to changes in ice retreat and advance (e.g. Arrigo et al., 2008; Pabi et al., 2008; Arrigo & van Dijken, 2011) thus making early spring (i.e. before or during ice retreat) and late fall (i.e. during or after ice advance) observations important. Increased duration of open water area has resulted in an increased importance of late season storms, which have been linked to both late season phytoplankton blooms (Ardyna et al., 2014) and CO_2 outgassing as a result of vertical mixing (Hauri et al., 2013; Evans et al., 2015).

Due to the difficult logistical nature of Arctic research, most Arctic inorganic carbon cycle studies focus on data from either summer or fall, and use data from other years to make assumptions about conditions outside of their observational window within the year of interest. However, the highly variable ice conditions (e.g. timing of retreat/freeze-up, extent, thickness, and concentration) between years could make such comparisons unrealistic. Several studies (e.g. Arrigo et al., 2015) have described the physical and biological transformations that occur between spring, summer, and fall within a year, but few have explicitly focused on the inorganic carbon system. Furthermore, only two field campaigns have characterized the carbonate system in spring, both of which were limited in spatial extent.

Here we present new biogeochemical data from the Chukchi Sea shelf and Canada Basin in spring, summer, and fall of 2014 and attempt to provide a synoptic view of the spatial and temporal controls on the carbonate system within one full ice melt season. Due to differences in the timing of the onset of ice melt between 2014 and earlier years, our work provides valuable insight into the importance of ice cover in setting the timing and magnitude of biological carbon cycling in the Chukchi Sea and Canada Basin. Furthermore, we evaluate air-sea CO_2 exchange between and within seasons and draw comparisons to previously published estimates of annual CO_2 uptake in the Arctic Ocean.

Chapter 2

STUDY AREA & METHODS

2.1 *Cruise Data*

Three research expeditions in 2014 (Figure 1) collected carbonate chemistry data in the western Arctic Ocean and are detailed below. Hydrographic data were collected in spring (15-May to 19-June) aboard USCG Icebreaker Healy during the SUBICE expedition in the Chukchi Sea. Heavy ice cover restricted the spatial extent of this cruise to a relatively small area of the Chukchi shelf. The CHINARE expedition aboard R/V Xuelong in summer (22-July to 29-August) collected data from the Bering Sea, Bering Strait, Chukchi Sea, Beaufort Sea, and Canada Basin. The R/V Mirai expedition in fall (3-28 September) collected data in the Bering Strait, central and northeast Chukchi Sea, and southeast Canada Basin. A fixed point observatory (FPO) was occupied between 6 – 25 September, with CTD casts around noon and midnight each day.

In spring, most of the 230 CTD stations were sampled for nutrients (NO_3^-, NO_2^-, NH_4^+, PO_4^-, $Si(OH)_4$), dissolved oxygen (DO), and chlorophyll *a* (chl *a*), while dissolved inorganic carbon (DIC) and total alkalinity (TA) data were collected from 69 stations. DIC and TA samples were collected into 250 mL borosilicate glass bottles, poisoned with 100 μL saturated $HgCl_2$ solution to prevent biological activity, sealed with Apezion high-vacuum grease and later shipped to the University of Southampton for analysis. DIC and TA samples were measured via coulometric and potentiometric titration using a VINDTA 3C (Marianda), with a precision of ± 2

μmol/kg^{-1}. Accuracy was verified using certified reference materials (CRMs) from Scripps Institution of Oceanography (SIO). Nutrient concentrations were determined using a Seal Analytical continuous-flow AutoAnalyzer 3 following a modified procedure after Armstrong et al. (1967). DO was measured using a spectrophotometer following the standard Winkler titration method, with a precision of ±1 μmol/kg^{-1}. Chl *a* measurements were made using a Turner 10-AU fluorometer (Turner Designs, Inc.) following the methods of Holm-Hansen et al. (1965) and were calibrated against a pure Chl *a* standard (Sigma). Nutrient, DO and chl *a* samples were measured onboard, while DIC and TA samples were measured at the University of Southampton, UK.

The summer expedition collected approximately 700 samples for DIC and TA from 74 stations using a 24-Niskin Seabird 911 CTD rosette. DIC and TA samples were collected similarly to the spring cruise, and were measured at the University of Delaware approximately four months after the end of the research expedition. DIC samples were analyzed using a LiCOR LI 7000 infrared CO_2 detector coupled to an automated DIC analyzer (Apollo SciTech, USA). TA samples were measured via open-cell potentiometric titration at 22° C with 0.1 M HCl^-. Precision of DIC & TA samples was within 0.1% (± 2 μmol/kg). Accuracy was verified using CRMs from SIO. Nutrient data were measured onboard using a San^{++} automated continuous flow autoanalyzer (SKALAR Inc.) following World Ocean Circulation Experiment protocols with a precision of ±0.03 μmol/kg. Chl *a* samples were collected for most stations and were measured following similar procedures to the spring expedition. DO was measured onboard using the spectrophotometric method based on Winkler titration with a precision of ±1 μmol/kg^{-1}.

In fall, hydrographic data were collected from 21 stations using a 36-Niskin Seabird 9plus CTD rosette. DIC and TA samples were collected following similar procedures to both the spring and fall expeditions. DIC samples were measured using an automated coulometric analyzer (Nippon ANS, Inc.) with a precision of ± 0.7 μmol/kg^{-1}. TA samples were measured using a custom spectophotometric system (Nippon ANS, Inc.) with a precision of ±0.57 μmol/kg^{-1}. Precision of DIC and TA samples was verified using CRMs from SIO. DO was measured via the spectrophotometric Winkler titration method (Kyoto Electronic Co. LTD), with a precision of ± 0.12 μmol/kg^{-1}. Chl *a* was measured using a fluorophotometer (Turner Designs) after Welschmeyer et al. (1994). Unfortunately, nutrient data are not yet available, so we consider the physical and biogeochemical controls on carbonate cycling using DIC, TA, DO, and chl *a* data.

2.2 *End-member mixing analysis*

In order to correct for changes to carbonate chemistry due to the effects of mixing between ice melt water, river water, and seawater, we employ a three end-member mixing model to estimate the fractions of each water mass in each sample. This method has been employed by several other investigators for similar studies in the Arctic Ocean (e.g. Yamamoto-Kawai et al., 2008; Jones et al., 2008; Cai et al., 2010) and is calculated as:

$$f_{IM} + f_{RW} + f_{SW} = 1 \quad (1)$$

$$f_{IM}S_{IM} + f_{RW}S_{RW} + f_{SW}S_{SW} = S_{obs} \quad (2)$$

$$f_{IM}TA_{IM} + f_{RW}TA_{RW} + f_{SW}TA_{SW} = TA_{obs} \quad (3)$$

Where *f* denotes fraction, IM denotes sea-ice meltwater, RW denotes river water, and SW denotes seawater. S_{obs} and TA_{obs} are the measured values of salinity and TA, respectively. We then extend this analysis to estimate quantify the contribution of biological changes to DIC by removing the effects of mixing:

$$(f_{IM}DIC_{IM} + f_{RW}DIC_{RW} + f_{SW}DIC_{SW}) + \Delta DIC_{OC} + \Delta DIC_{air-sea} = DIC_{obs} = \Delta DIC_{mix} + \Delta DIC_{OC} + \Delta DIC_{air-sea} \quad (4)$$

Rearranged to estimate the biological contribution to DIC in any sample,

$$\Delta DIC_{OC} = (\Delta DIC_{obs} - \Delta DIC_{mix}) - \Delta DIC_{air-sea} \quad (5)$$

The S (= 32.6 PSU), TA (= 2211 μmol/kg^{-1}) and DIC (2148 μmol/kg^{-1}) end-members for seawater were selected from averaged values of upwelled Bering Sea slope water during summer 2014 as this is the source of waters entering the Arctic Ocean through the Bering strait. End-member values (S = 4 PSU; TA = 360 μmol/kg^{-1}, DIC = 320 μmol/kg^{-1}) for ice-melt are based on values reported by Rysgaard et al. (2007), while end-member values for river water (S = 0; TA = 1300 μmol/kg^{-1}, DIC = 1350 μmol/kg^{-1}) are similar to those reported by Cooper et al. (2008) for the flow-weighted averages of the Yukon and Lena rivers, which most likely had the strongest influence on our measurements due to their proximity to our study area.

2.3 *Salinity Normalization*

In order to compare our results between cruises, which encountered a wide range of salinity values, we normalize our DIC and TA data as described by Friis et al. (2003). Given the abundance of river inflow in our study area, we normalize using the DIC, TA, and S concentrations of river water in our end-member mixing analysis:

$$nDIC = \left(\frac{DIC_{obs} - DIC_{RW}}{S_{obs}} S_{ref}\right) + DIC_{RW} \quad (6)$$

$$nTA = \left(\frac{TA_{obs} - TA_{RW}}{S_{obs}} S_{ref}\right) + TA_{RW} \quad (7)$$

where *n*DIC and *n*TA are normalized DIC and TA, respectively; DIC_{obs}, TA_{obs}, and S_{obs} are measured DIC, TA, and salinity, respectively. DIC_{RW} and TA_{RW} are the chosen end-member values for river water in the Arctic, respectively. S_{ref} refers to S = 33.1, which is representative of the core of the lower halocline layer (LHL) in the western Arctic, which is usually found ~150 m.

2.4 *Air-sea CO_2 fluxes*

To calculate air-sea CO_2 fluxes, we used pCO2 calculated from measured DIC and TA data combined with wind speeds from Point Barrow, AK measured by the NOAA Earth System Research Laboratory (ESRL) (http://www.esrl.noaa.gov/gmd/obop/brw/). Four different wind speeds were applied: daily average for each sample collection date, seasonal (May – September) average, seasonal minimum, and seasonal maximum. The sea-air flux of CO_2 (F_{CO2}; in mmol m^{-2} d^{-1}) was calculated according to:

$$F_{CO2} = ks(\Delta pCO_2) \quad (8)$$

where k is the gas transfer velocity of CO_2 (cm h^{-1}), s is the solubility of CO_2 (mol L^{-1} atm^{-1}), and ΔpCO_2 is the difference between calculated seawater pCO_2 and measured atmospheric pCO_2. Negative F_{CO2} values indicate a flux of CO_2 from the atmosphere into the surface ocean. We calculated k following the parameterization of Ho et al. (2006):

$$k = 0.31u^2(Sc/600)^{-0.5} \quad (9)$$

where u is wind speed (m sec^{-1}) at 10 m and Sc is the Schmidt number, calculated from sea surface temperature after Wanninkof et al. (1992). Daily average atmospheric pCO_2 values were downloaded from NOAA ESRL (http://www.esrl.noaa.gov/gmd/obop/brw/). Given that sea ice is known to be an imperfect, but relevant barrier to gas transfer (Bates et al., 2014; Loose et al., 2011) we apply a linear correction to all measurements where sea ice was present following the methods of other studies (e.g Bates, 2006; Gao et al., 2012). For example, for a station where 60% ice cover was present, we multiply the calculated air-sea pCO_2 flux by 0.4.

In order to estimate total seasonal CO_2 uptake, we first take average flux estimates for all stations during each study period and extrapolate them to the entire 595,000 km^2 Chukchi shelf. For gaps between observational periods (e.g. between the end of spring measurements to the beginning of summer measurements), we assume a

linear surface pCO_2, temperature, salinity, and ice concentration change between each observation and calculate new air-sea fluxes using each different set of wind speeds similarly to Jiang et al. (2008). We consider the end of the ice retreat/phytoplankton growing season to be the date at which ice fully covered the Chukchi shelf, which we set to 15-Dec. based on satellite ice concentration images obtained from http://www.iup.uni-bremen.de/. Since no pCO_2 measurements are available from the end of our fall observations to the date of 100% ice cover, we apply our linear interpolation between average fall pCO_2 and average early spring pCO_2 measurements under 100% ice cover.

2.5 *Satellite ice concentration and primary productivity estimates*

We use satellite estimates of ice concentration (%), chl *a* (mg m^{-3}), and daily primary productivity (mg C m^{-2} day^{-1}) as a supplement to interpret our *in situ* measurements. Data were processed and shared by the Arrigo Ocean Biogeochemistry lab at Stanford University. Ice concentration data are based on the SSM/I Sea Ice Concentration NASATeam algorithm (see https://nsidc.org/data/docs/daac/nasateam/). Chl *a* data are based on 8-day level 3 binned measurements from the MODIS radiometer onboard NASA's Aqua satellite. Primary productivity was estimated as described in Pabi et al. (2008). Estimates are reported as 5x5km averages surrounding the nearest hydrographic station location.

2.6 *Data Reporting*

Given the multitude of variables considered in this work, we mostly report temperature, salinity, pCO_2, ΔDIC, AOU, NO_3^- and chl *a* values in our discussion of

the spatial and temporal controls on carbonate chemistry between and within seasons. The reader is referred to the referenced summary tables for consideration of other important associated biogeochemical parameters. Values are mostly reported as mean ± standard deviation, while ranges are left to summary tables. Associated carbonate system variables in addition to measured DIC and TA were calculated with the CO2SYS program using the constants of K_1, K_2 from Mehrbach et al., (1973) as refit by Dickson and Millero (1987). For mixed layer estimations, we define the base of the surface mixed layer as the depth at which density (σ_Θ) is 0.05 kg m^3 greater than surface measurements.

Chapter 3

RESULTS

3.1 *Chukchi Shelf observations (Spring)*

Ice melt in the spring study area was delayed compared to previous years due to persistent northerly winds and a late season snowfall, resulting in cooler temperatures and reduced light transmission to under ice water (SUBICE cruise report). Most CTD stations were located between 70 – 73.3° N (hereafter referred to as the study area) and were heavily ice-covered. Only 6 stations were occupied with ice concentrations <65%, which were in the southern Chukchi Sea (<69.5° N; hereafter referred to as S. Chukchi stations). These stations were warmer, fresher, and of lower pCO_2 (306 ± 85 μatm) than the study area, indicating the presence of Pacific Summer Water (PSW; a blend of Alaskan Coastal Water [ACW], Bering Sea Water [BSW], and/or Anadyr Water; Table 1). Most stations in the study area were fully mixed, and exhibited a narrow range of physical and biogeochemical water properties (Table 1). Ice melt began in the southern portion of the study area around or after 5 June, as evidenced by slight warming and freshening of surface samples. Due to differences in physical and biogeochemical parameters that were apparent after 5 June, we divide our analysis of the study area into early spring (15 May – 4 June) and late spring (5 – 19 June) periods. We also consider stations on the NE Chukchi slope separately due to their closer resemblance to Beaufort Gyre/Canada Basin water.

In early spring, a substantial fraction of remnant Pacific Winter Water (PWW; S>32.5 PSU, T<-1.6° C) was evident, as confirmed by negative *f*SIM values, which

indicate brine rejection during sea ice formation (Table 1). In general, a very narrow range of temperature and salinity values were observed. Small differences between surface and bottom water were evident, and salinity was slightly lower in the northern study area, potentially due to advection of BSW (S<32.5 PSU; T>1.6° C; Figure 2a,b) Lower salinity and warmer water was observed in both the eastern and western extremes of the study area, which suggests the presence of inflowing ACW and BSW, respectively. High pCO_2 (607 ± 130 µatm), AOU (42.8 ± 17.3 µmol/kg^{-1}) and NO_3^- (11.6 ± 2.4 µmol/kg^{-1}) values were observed (Table 1 and Figure 2c,d,f). Most early spring stations had low chl *a* concentrations (~0.55 mg m^{-3}), but relatively high concentrations (5-9 mg m^{-3}) were found in the southeast near the Alaskan coast on 18 May where the first signs of ice melt were evident (Figure 3e,h). High ΔDIC values were found north of 71° (Figure 2g).

In late spring, warming and freshening occurred between ~69.5° – 71° N, with T-S properties indicative of mixing between PWW, ice melt, and advected PSW (Figure 3 a,b). Ice concentrations around ~70° N had decreased by 50-60%, while little to no melting was evident in the majority of the study area (i.e north of 71°; Figure 3h). Ice melt around 70° N correlated with a large expansion of the initial early spring bloom, with chl *a* concentrations up to ~20 mg m^{-3} and satellite productivity estimates of ~269 mg C m^{-2} day^{-1} (Figure 3e). Preliminary data suggest that NO_3^- uptake rates were highest here, whereas low rates were observed at stations under heavy ice cover (SUBICE cruise report). Outside of this bloom, a patchy distribution of elevated surface and subsurface chl *a* was observed in the central study area below 72° N, ranging from 0.9 – 14.8 mg m^{-3} (Figure 3e). However, in this area, a weak relationship between chl *a* concentrations, DO production, and CO_2 and nutrient

uptake is apparent. Outside of the bloom at 70° N, the dominant changes to the carbonate system were mixing between PWW and upstream Bering Sea water, with lower nutrient concentrations and pCO_2 due to earlier biological activity in the southern ice-free region (Figure 3c,d,f). High ΔDIC values north of 72° were evident where ice cover remained heavy (Figure 3g). In some cases, evidence for benthic accumulation of chl *a* was found, with higher bottom concentrations than at the surface. These accumulations were found where ice had melted in the later portion of the cruise around 70° N. High concentrations of ice algae were observed at most stations in the cruise (SUBICE cruise report), which could potentially explain the benthic accumulations associated with ice melt.

3.2 *Chukchi Shelf observations (Summer)*

Spatial differences in carbonate system distributions during our summer observations are summarized in Table 2. Between spring and summer, ice had melted completely in the spring study area, and the ice edge was located around 73-75° N (Figure 4h). Ice concentrations on the northern shelf ranged between 18-58%, with heavy ice cover restricted to the Canada Basin. Mixed layer temperature and salinity correlated with ice concentration on the shelf, with warmer and saltier water in the southern ice-free study area, and colder and fresher water in the actively melting northern study area (Figure 4a,b; Table 2). Average mixed layer depths were shallower in the marginal ice zone (7 m) than the ice-free southern study area (15 m) due to freshwater stratification from the addition of ice melt and river water in the north.

Between spring and summer, the widespread distribution of remnant PWW in spring was mostly replaced by warmer, fresher, and lower pCO_2 PSW in summer. The fully mixed water column representative of early spring conditions transitioned to a shallow, warm, and fresh surface mixed layer above a sharp pycnocline (Figure 4a,b). The largest changes to the carbonate system occurred in the ice-free shelf region, where widespread reductions in pCO_2 occurred between spring and summer (Figure 4c). Satellite productivity estimates in this region ranged from 216 – 1260 mg C m^{-2} day^{-1}, with decreasing productivity in the north, where the least amount of time had elapsed since ice retreat. Surface pCO_2 showed a similar trend, but also increased to near atmospheric values near the Alaskan Coast, where a higher *f*RW demonstrated the influence of high pCO_2 river water. NO_3^- values were extremely low, and were depleted throughout the entire water column on the central Chukchi shelf (Figure 4f). Very low ΔDIC values (<250 μmol/kg^{-1}) were observed in the southern Chukchi Sea, (Figure 4g).

Subsurface samples at ice-free stations were slightly cooler and saltier, and had slightly higher pCO_2 (256.1 ± 92.6 μatm) than mixed layer samples (Table 2; Figure 4c). Slightly higher average chl *a* concentrations (2.1 ± 3.1 mg m^{-3}) were found between 20-50 m depth, characteristic of the subsurface chlorophyll maximum (SCM) that is commonly observed during summer (Martin et al., 2010). Further evidence of the benthic accumulation of sinking biomass was observed, with high chl *a* concentrations found on the benthos (up to 8.9 mg m^{-3}). ΔDIC values were slightly lower than in the surface, while AOU values were slightly higher (Table 2).

Compared to ice-free stations, biological CO_2 uptake was restricted to <10 m in the actively melting zone. Very low surface pCO_2 and AOU values (124 – 240

μatm; -140 to -113 μmol/kg^{-1}, respectively) in the melting zone were observed, but increased rapidly corresponding to a shallow nutricline (Figure 4c,f). PWW, which had disappeared from most of the shelf between spring and summer, remained present at ice edge stations between 50-150 m. Both *f*SIM and *f*RW values increased between spring and summer due to the retreat of sea ice and increased river discharge (Figure 4h). Surface ΔDIC was very low (-215 μmol/kg^{-1}) and correlated with high concentrations of chlorophyll at the ice edge (Figure 4e,g,h).

3.3 *Canada Basin Observations (Summer)*

Unfortunately, a lack of spring measurements due to heavy ice cover in the Canada Basin limits our comparison over the broad geographical range covered in summer. A summary of the physical and biogeochemical distributions relevant to the carbonate system can be found in Table 3. Between spring and summer, ice retreated into the Canada Basin, with intermediate ice cover (15 – 56%) between 72 – 76° N, and heavy ice cover (65 – 100%) between 76 – 81° N (Figure 5h). Mixed layer depths increased with increasing ice cover, averaging 8.4 ± 3.8 m between 72 – 76° N, and 14.6 ± 5.0 m between 76 – 81° N. No significant differences in physical and biogeochemical parameters were evident between these two zones, nor were any latitudinal or longitudinal trends observed in mixed layer pCO_2. Mixed layer samples in the Canada Basin were cold and fresh, with higher pCO_2 (290 ± 26.7 μatm) than ice-free shelf stations (Figure 5a,b,c). Very low nutrients (NO_3^- <0.4 μmol/kg^{-1}) and chl *a* concentrations (<0.2 mg m^{-3}) were observed at most stations (Figure 5e,f). Average ΔDIC and AOU values (-38 ± 16 and -12.5 ± 18.4 μmol/kg^{-1}, respectively; Table 3) were higher than the shelf, but lower than those observed under heavy ice

cover in spring. *f*SIM and *f*RW values were high (0.09 ± 0.02 and 0.07± 0.01) compared to spring values. In general, mixed layer samples in summer exhibited a much smaller undersaturation in surface pCO_2 and nutrients than shelf stations.

The presence of PSW was evident at all stations of the Canada Basin, evidenced by a local temperature maximum at a depth range of 30 – 58m (Table 3). pCO_2 values in this water mass were similar to the surface mixed layer (291.5 ± 30.8 µatm), and the highest chl *a* concentrations among all basin samples were found in this water mass (0.3 ± 0.3 mg m^{-3}) due to the widespread occurrence of a SCM. Average ΔDIC was lowest in this water mass (-72.0 ± 20.6 µmol/kg^{-1}), but AOU values were similar to the mixed layer (-15.4 ± 21.4 µmol/kg^{-1}; Table 3). Compared to spring measurements, the depth of the nutricline in the Canada Basin had deepened, from ~25 m in May to as deep as 60 m in July. Between 60-100 m in both spring and summer, pCO_2 increased rapidly, corresponding to the upper halocline layer as evidenced by negative fSIM values due to the presence of remnant PWW. ΔDIC increased sharply, and in some samples was positive, indicating that respiration was producing CO_2 in the halocline.

3.4 2014 Fall Observations

We divide our description of this cruise into three main sections: Southern Chukchi Sea (65.7° – 68° N), Chukchi shelf (69° – 74° N) and NE Chukchi Sea/Canada Basin (74.4° – 75.1° N) (Figure 1). At this time, ice had retreated further into the Canada Basin, with the marginal ice zone located around 76° N. A summary of the physical and biogeochemical distributions relevant to the carbonate system can be found in Table 4.

3.4a *Southern Chukchi Sea*

Three stations in the southern Chukchi sea were occupied on 3-Sept. (hereafter early fall), at the beginning of the cruise. The weak density stratification that was apparent in early summer had strengthened by early fall, with a 20 m surface PML separated from subsurface BSW. Chl *a* values increased in the upper 20 m from ~1.5 – 19 mg m^{-3} in summer to 3.7 – 32 mg m^{-3} in early fall, which were the highest values observed in the entire growing season. Satellite chl *a* measurements yielded productivity estimates of 1436.8 ± 282.3 mg C m^{-2} day^{-1}. However, pCO_2, AOU and ΔDIC values increased at nearly all sample depths between late July – early September, while DO values decreased (Table 3; Figure 6 c,d,g). Both *f*SIM and *f*RW were <0.04 and 0.001, respectively, during both observations.

When this area was revisited 25 days later, the high chl *a* present in early September had essentially disappeared, as evidenced by reductions in chl *a* concentrations and satellite-derived productivity estimates, which decreased from 1436.8 ± 282.3 mg C m^{-2} day^{-1} to 310.6 ± 83 mg C m^{-2} day^{-1}. pCO_2 had increased in at all depths except at 30 m.

3.4b *Chukchi Shelf*

Between summer and fall, slightly cooler and fresher water filled the upper ~30 m of the shelf between ~70 – 73° N (Figure 6a,b). Both *f*SIM and *f*RW values were generally <0.06 on most of the shelf, but increased rapidly above 73° N (up to 0.16 and 0.09, respectively). Between 72.7 - 74° N, a distinct freshwater front separated the PML from colder, fresher Canada Basin water, which shoaled the mixed layer from 30 m in the south to <10 m in the north (Figure 6a,b). A strong pycnocline

was present, which isolated the low pCO_2 (~240 μatm) PML from higher pCO_2 subsurface PSW (Figure 6c). The ice-free areas of the shelf in summer had higher pCO_2, AOU and ΔDIC values in the fall (Tables 3,4; Figure 6c,d,f). However, the zone of low surface pCO_2 at the ice edge in summer (i.e between 73 – 74° N) had deepened from <10 m in summer to ~30 m in fall (compare Figs. 4 and 6), with mild increases in DO observed as deep as 50 m. Interestingly, the disappearance of the high chl *a* concentrations associated with the ice edge in summer appears to correlate with a strong increase in pCO_2 between 75 – 100 m in fall (Figure 6c).

3.4c *NE Chukchi Sea/Canada Basin*

Samples were collected twice daily between 6 - 25 September at a fixed point on the NE Chukchi slope/SE Canada Basin, with bottom depths between 1077 – 2057 m (Figure 7). Strong surface stratification due to freshwater addition via ice-melt, river input, and the influence of the Beaufort Gyre was prevalent throughout the observation period (Figure 7). Over the course of sampling, the addition of ice-melt and river water slightly decreased surface temperature and salinity, deepening the $\sigma_\Theta = 23$ isopycnal from ~10-15 m to 20 m (Figure 7a,b,). Mixed layer *f*SIM and *f*RW were both high, and similar to summertime observations nearby (0.14 ± 0.02 and 0.05 ± 0.02, respectively). This area was under intermediate ice cover in August, and showed an increase in surface pCO_2 since then (319 ± 15.1 μatm), and a moderate increase over the course of the sampling period (Figure 7c). In general, chl *a* concentrations were low (~0.5 mg m^{-3}; Figure 7e), but showed spatial differences during the study period. In the first week of sampling, the highest mixed layer chl *a* concentrations correlated with the lowest pCO_2 concentrations (Figure 7c,e). The lowest ΔDIC values

were similarly observed during this time (Figure 7f). Between 11-17 Sept., elevated chl *a* values were found beneath the mixed layer, and had reduced to <0.15 mg m^{-3} in the surface layer. During this time, surface pCO_2 peaked, reaching 362.9 μatm, and remained >294 μatm for the remainder of the study (Figure 7c). Between 14 – 25 Sept., *f*RW increased steadily, from ~0.04 to 0.09, while *f*SIM peaked at 0.16 on 17 – Sept. and decreased afterwards.

Between 20-55 m, a subsurface pCO_2 and AOU minimum was present, corresponding to elevated chl *a* concentrations (0.08 – 0.99 mg m^{-3}; Figure 7c,d). The pCO_2 minimum observed here persisted throughout the duration of the study, but was only slightly lower than the mixed layer (299.5 ± 13.9 μmol/kg^{-1}). AOU values were significantly lower than surface values (-26.8 ± 6 μmol/kg^{-1}). This weakly productive layer shrank in areal extent following the small surface chl *a* bloom that was present on 10-11 September. Over the course of the study, no trend was apparent in either subsurface pCO_2 or DO, suggesting that the activity of the SCM remained constant.

3.5 *Air-sea CO_2 fluxes*

Air-sea CO_2 fluxes calculated at each different wind speed for each study period are summarized in Table 5, and we henceforth discuss our results using seasonally averaged wind speeds (5.8 m sec^{-1}). The use of daily wind speeds can result in large over- or underestimations of air-sea CO_2 flux due to the high sensitivity of flux calculations to wind speed, which can be highly variable (Evans et al., 2015). The Chukchi shelf acted as a sink for atmospheric CO_2 during all study periods except early spring, and exhibited large variability depending on the time of observation. The early spring study period exhibited the smallest average F_{CO2}, ranging from -9.0 to 4.4

mmol m^{-2} d^{-1}, with the strongest uptake occurring in the ice-free southern Chukchi shelf.

In late spring, the average strength of the Chukchi shelf F_{CO2} uptake increased, and ranged from -7.9 to 1.9 mmol m^{-2} d^{-1}. The strongest uptake during this time period occurred at the ice edge, with F_{CO2} values ranging from -2.8 to -5.7 mmol m^{-2} d^{-1}. As ice melted further between late spring and summer, our linear interpolation of F_{CO2} results in a continued increase in the strength of the Chukchi shelf carbon sink at a rate of -0.46 mmol m^{-2} d^{-1}.

Air-sea CO_2 flux was strongest during summer, ranging from -23.4 to -2.9 mmol m^{-2} d^{-1}. We observed the strongest F_{CO2} in the ice-free southern Chukchi shelf and in the marginal ice zone between 71 – 72° N, just south of the ice edge. Notably, the weakest CO_2 uptake was observed on the central shelf between 68 – 70° N. F_{CO2} at ice covered (18 – 58%) stations was variable (-32.1 to -5.1 m^{-2} d^{-1}), with the strongest sinks occurring at the ice edge. Between our summer and fall observations, our linear interpolation shows a continued uptake of CO_2 on the shelf, but at a slower rate (-0.08 mmol m^{-2} d^{-1}) compared to between spring and summer.

During fall, the strong uptake rates were observed, with central shelf (67 – 72.8° N) values ranging from –18.0 to -12.7 mmol m^{-2} d^{-1}. At the location of the ice edge during summer, F_{CO2} had decreased to a range of -14.9 to -6.4 mmol m^{-2} d^{-1}. During the ice advance period (i.e 28-Sept. to 15-Dec.), F_{CO2} decreased at a rate of 0.15 mmol m^{-2} d^{-1}.

Chapter 4

DISCUSSION

4.1 *Shelf Ice edge vs. Under ice blooms*

Our results demonstrate the importance of the timing of sea ice retreat in controlling the distribution of carbonate parameters in spring and summer, and allow us to draw conclusions about whether or not the biological controls on carbonate distributions follow those of ice edge blooms or under ice blooms. Perette et al., (2011) describe the classic view of the seasonal evolution of Arctic biological productivity as follows: as ice retreats from the Bering Strait towards the Canada Basin, phytoplankton communities proliferate along the ice edge, consuming nutrients due to the release of light limitation. These authors liken the evolution of the system to a wave-like propagation, with the consumption of surface nutrients in the weeks following ice retreat resulting in the migration of phytoplankton to deeper depths to consume nutrients in the nutricline. Arrigo et al. (2015) suggest this longstanding paradigm may need to be revised due to the discovery of massive concentrations of chl *a* under heavy sea ice cover in 2010 and 2011 by Arrigo et al. (2012). Lowry et al. (2014) discuss the distributions of these different blooms types (i.e ice edge vs. under ice), and suggest that such under ice blooms are widespread, and constitute a much larger areal fraction of primary productivity than the ice edge blooms described by Perette et al. (2011). The purpose of the spring 2014 SUBICE cruise in spring was to test the hypothesis that under ice blooms were the dominant feature of early season primary productivity.

Ice retreat began 1 – 2 months later in 2014 than in 2008, 2009 and 2012 (Perovich et al., 2012; Fujiwara et al., 2014; Figure S1), and was characterized by the presence of thick, multi-year ice and heavy snow cover. In early spring, biological CO_2 uptake was highest where sea ice had been absent for ~14 days (i.e S. Chukchi Sea), and at the ice edge at ~ 70° N on the Chukchi shelf (Table 1). Where ice cover remained high, reduced light transmission limited the onset of biological productivity, as evidenced by low NO_3^- uptake rates and the absense of chl *a* (Figure 2; SUBICE cruise report). North of 71°, high ΔDIC confirm the absence of under-ice biological CO_2 fixation (Figure 2). Between early and late spring, further ice melt to ~ 71.5° N correlated with an expansion in the areal extent of biological pCO_2 uptake, with a reduction of surface pCO_2 and NO_3^- to <255 µatm and <0.05 µmol/ kg^{-1} between the two study periods (Figure 3c,f). Above 71.5° N, where ice cover remained high, pCO_2 and NO_3^- remained high (>570 µatm and >13 µmol/ kg^{-1}, respectively). ΔDIC values showed similar distributions, further suggesting that biological productivity was restricted to the ice edge. Under heavy ice cover (i.e > 71.5° N), changes in pCO_2 and NO_3^- appeared to correlate more closely with changes in temperature and salinity between early and late spring, suggesting that the advection of PW played a more important role in setting carbonate distributions during this time. Therefore, biological productivity played a role in CO_2 uptake only where ice cover retreated in both early and late spring.

A comparison of representative station profiles from the southern Chukchi Sea, central Chukchi shelf, and NE Chukchi Sea illustrates the influence of the timing on sea ice retreat on biogeochemical cycling over the course of the growing season (Figures 8-10). We observed the largest magnitude of changes to the carbonate system

in the southern Chukchi Sea, which had been ice free for ~14 days at the start of spring observations (Figure 8b,c,d). This region experienced the longest duration of open water, and experienced a smaller influence of freshening due to ice melt as a result of mixing via the persistently strong advection that occurs through Bering Strait. Strong surface biological DIC removal between spring and summer was followed by strong subsurface biological DIC addition between summer and fall due to remineralization of OM produced earlier in the season (Figure 8c). This pattern is consistent with several previous observations (e.g. Bates et al., 2009; Nishino et al., 2015). However, when compared to data from 2012, distinct differences are apparent between summer and fall 2012 pCO_2 values, with low pCO_2 (~185 μatm) throughout a well mixed water column in summer and extremely high pCO_2 (1972 μatm) between 40 – 50 m in fall. We attribute these differences to a longer ice free period in 2012, which allowed for an earlier accumulation and subsequent recycling of surface derived OM.

Further north on the central shelf, we observed post-bloom conditions, with widespread reductions in pCO_2, nutrients, and chl *a*, consistent with other reports of summer conditions on the Chukchi shelf (e.g. Bates et al., 2006; Pabi et al., 2008; Forest et al., 2014). Here, low pCO_2 was observed as deep as 40 m in summer, which had only increased slightly in the fall due to a shorter duration of ice free conditions (Figure 9b). Between summer and fall, subsurface ΔDIC values increased by ~100 μmol/kg^{-1}, and pCO_2 increased from ~200 to 350 μatm due to biological DIC addition. In 2012, subsurface pCO_2 values >560 μatm were already observed in this area at a similar time due to the earlier retreat of sea ice and thus an earlier switch from net biological removal to net addition of CO_2.

The very low surface pCO_2 we observed at the ice edge in summer around 73 – 75° N followed a seasonal trend characteristic of the ice edge blooms discussed by Perette et al. (2011) and Hill and Cota (2005). In summer, low pCO_2 values were co-located with high chl *a* values at the ice edge, but were restricted to <10 m (Figs. 4c,e, 10 b,f). Very low surface ΔDIC values (<215 μmol/kg^{-1}) confirm that biological consumption of CO_2 at the ice edge was the dominant control (rather than freshwater dilution) on pCO_2 undersaturation here (Fig. 10c). In the weeks following continued ice retreat, strong surface stratification allowed for this zone of low pCO_2 to deepen to ~35 m (Figs 6c, 10b). This stratification allowed the phytoplankton community to consume the abundant nutrients available in summer, deepening the nutricline to >40 m in fall. In fall, a well-developed SCM was apparent below the mixed layer, which had reduced pCO_2 and AOU significantly between summer and fall (Figure 10b,e). The activity of the SCM on the Chukchi shelf is consistent with the findings of Brown et al. (2015), who showed that the SCM actively consumes nutrients in the nutricline following ice retreat. However, the SCM only showed signs of net productivity in the north, where a minimal amount of time had elapsed between summer ice retreat and our fall observations. Further south, higher subsurface pCO_2 and AOU values suggest that any SCM productivity was balanced by subsurface OM remineralization.

The pCO_2 distributions we observed followed a wave-like propagation similar to that described by Perette et al. (2011) for productivity at the ice edge (compare Figs. 4 and 6). In the southern Chukchi Sea, longer ice-free conditions allowed for the earliest onset of summer biological production and subsequent fall subsurface OM remineralization. On the central shelf, where only weeks had elapsed since ice retreat, pCO_2 values remained undersaturated with respect to the atmosphere, and only

minimal subsurface remineralization had begun to occur between summer and fall. At the ice edge in summer, no remineralization signature was apparent; rather, the depression of the nutricline into late fall after stratification is more representative of the post-bloom conditions that were apparent further south in the summer. Arrigo et al. (2015) suggest that under ice blooms reduce nutrients (and thus pCO_2) in the upper water column weeks before ice melt occurs. If that were the case, the zone of low pCO_2 and nutrients should have been substantially deeper at the time of our summer observations. Instead, we observed low pCO_2 and nutrients only in the upper ~10 m at the ice edge, with high concentrations directly below (Figure 4). Furthermore, we found no evidence of under ice blooms during spring, and found that biological productivity was restricted to the location of the ice edge. The late spring snowfall that occurred may be responsible for the lack of an under ice bloom, as Zhang et al. (2015) showed that snowfall reduced light transmission through sea ice and can thus impact nutrient availability in spring.

4.2 *Canada Basin carbonate distributions*

In the Canada Basin, our spring measurements suggest that the biogeochemical starting conditions are vastly different from those on the shelf, owing to low bacterial respiration during the winter (Wiebe et al., 1992). The minimal change in mixed layer pCO_2 we observed between spring and summer in the Canada Basin (Tables 1, 2; Figure 5) is consistent with previous reports that ice retreat beyond the shelf break results in only weak atmospheric CO_2 uptake due to persistently oligotrophic conditions and strong freshwater stratification (Cai et al., 2010; Else et al., 2013). Compared to summer 2008, when ice retreat had begun ~1-2 months earlier (Fujiwara

et al., 2014), we observed intermediate ice cover (15 – 50%) at 72 – 76° N, whereas this region was ice free in summer 2008. We observed lower pCO_2 (~290 µatm) in this region in 2014 compared to 2008 (~330 µatm), which we attribute to atmospheric CO_2 invasion following ice retreat in 2008. Interestingly, lower pCO_2 was found in the northern region in 2008 (i.e > 76° N at the ice edge) than in 2014. Coupel et al. (2012) report the presence of pelagic diatoms in this region in 2008, which were likely associated with the marginal ice zone. Therefore, it is likely that the lower pCO_2 values found in 2008 in the high latitudes were due to biological productivity occurring farther north near the ice edge. The dominance of prasinophytes, rather than diatoms, between 72 – 76° N in 2008 suggests that phytoplankton communities shift to smaller celled, less productive cells following disappearance of the initial larger, more productive cells after ice fully melts (Coupel et al., 2012; Fujiwara et al., 2014). Therefore, as ice retreated beyond 76° N in late summer 2014, it is likely that some further drawdown of atmospheric CO_2 occurred due to short-lived productivity following the ice edge. However, the shorter duration of open water in 2014 compared to 2008 would suggest that a smaller total uptake of atmospheric CO_2 would have occurred.

Data from the FPO between 5 – 25 Sept. shows how only minimal biological productivity occurs in the Canada Basin in fall, but does play a role in controlling surface pCO_2 (Figure 7). The increase in pCO_2 following the disappearance of surface chl *a* shows that the minimal early biological CO_2 uptake was balanced by atmospheric CO_2 intrusion, and thus shows the Canada Basin acts as a weak CO_2 sink even in fall. The distribution of chl *a* during this time is interesting given its apparent migration below the mixed layer following the initial surface concentrations of ~0.9

mg m^{-3}, and its subsequent reappearance in the surface towards the end of the study period (Figure 7e). The reappearance of surface chl *a* correlates with AOU and *f*RW, both of which increased steadily in the upper 10 m after 11-Sept. Brown et al. (2015) discuss the counterintuitive existence of surface chl *a* where nutrients are exhausted, and suggest that such a phenomenon could be due to the existence of small, slowly sinking cells fueled by regenerated NH_4^+. Such a scenario could plausibly explain our measurements, and would suggest that small phytoplankton most likely play a key role in maintaining slight, but undersaturated pCO_2 conditions in the basin following ice retreat in the oligotrophic Canada Basin. Over the course of the FPO, we observed persistently low subsurface pCO_2 beneath the mixed layer due to the presence of the SCM. (Figure 7c). Average pCO_2 values (297.3 ± 12.7 μatm) were remarkably similar to the SCM values observed in the Canada Basin during summer (293.6 ± 40.2 μatm), but the depth of the SCM was slightly shallower in fall. Additionally, average pCO_2 values at the SCM in summer 2014 were only slightly higher than in 2008 under low ice cover (280.3 ± 34.9 μatm). This finding suggests that increased light transmission following ice retreat in the basin had only minimal influence on the productivity of the SCM. In both seasons, the co-location of the SCM at the beginning of the nutricline, well below the mixed layer, is notable for two reasons. First, if the SCM is responsible for a large fraction of the biological CO_2 fixation in the Canada Basin, its isolation from the mixed layer means it is not an important contributor to atmospheric CO_2 uptake. Second, if the SCM sets the upper limit for vertical nutrient diffusion (Martin et al., 2010), then increased biological productivity in a future ice free Canada Basin due to increased wind-induced vertical mixing could be subdued. More research into the productivity of the SCM and its influence on CO_2 cycling is needed, but it is likely

that the SCM could have important implications for future carbon cycling in the Canada Basin.

4.3 *Seasonal air-sea CO_2 fluxes*

Air-sea CO_2 flux rates during our observations demonstrated high spatial and temporal variability (Table 5). During early spring, the Chukchi shelf acted as a net, albeit weak source of CO_2 to the atmosphere. Other studies have reported similar values for winter-spring CO_2 efflux (Semilitov et al., 2007; Evans et al., 2015) and attribute this result to the dominance of net remineralization during winter causing strong seawater pCO_2 supersaturation. In both early and late spring, the strongest air-sea CO_2 fluxes correlated with ice-free or ice-edge areas where evidence of biological productivity was observed. During summer, our results are consistent with the findings of other authors (e.g. Pipko et al., 2002; Bates, 2006; Bates et al., 2012), who attribute very strong air-sea CO_2 flux to strong seawater pCO_2 undersaturations owing to high rates of biological productivity following ice retreat (Hill & Cota, 2005; Carmack & Wassman, 2006). We observed very strong rates of air-sea CO_2 flux during all seasons in the southern Chukchi sea, which is a persistent biological hotspot over the course of the ice-free season due to the continuous supply of nutrient-rich Pacific water through Bering Strait (Springer & McRoy, 1993; Nishino et al., 2015). We also observed strong air-sea CO_2 flux at the ice edge in both spring and summer, which is consistent with the pattern of biological productivity occurring at the ice edge as it retreats north each season (Pipko et al., 2002; Perette et al., 2011).

Air-sea CO_2 flux rates demonstrate a wide variability between different studies (Table 6; references therein) and result in uncertainties for a number of reasons. The choice of wind speeds (e.g. instantaneous, daily/monthly/seasonally averaged) can

result in a large variability in flux calculations, as well as the use of different wind speed parameterizations (Evans et al., 2015). Most studies extrapolate their measurements to an assumed ice-free season of 100 days (e.g. Bates, 2006; Gao et al., 2012), but recent changes to both the timing and magnitude of ice retreat could add uncertainty to such an assumption. Furthermore, the timing of observations could result in measurements occurring before or after peak air-sea CO_2 exchange. Additionally, the linear correction for gas exchange through ice may not be representative of reality, as it is still unknown to what degree ice cover controls pCO_2 flux (Rysgaard et al., 2011; Loose et al., 2012).

Our results highlight the importance of the timing of observations on estimations of seasonal air-sea CO_2 exchange and therefore total seasonal CO_2 uptake. The large variability in measured and predicted F_{CO2} during each time period in Table 4 demonstrates the large range of seasonal CO_2 uptake estimates that would be predicted if measurements were restricted to one particular observational period. Most importantly, our results demonstrate the importance of using multiple seasonal observations to estimate total CO_2 uptake. By combining our spring, summer, and fall F_{CO2} measurements with linearly interpolated estimates of air-sea CO_2 flux using seasonally averaged wind speeds, we predict a total Chukchi Sea seasonal uptake of 7.7 Tg C (Tg = 10^{12} g). Using the approach commonly employed in other published literature, extrapolation of our summer or fall measurements to 100 ice-free days would yield estimates 2.1 and 2.5 Tg C higher, respectively, than our full seasonal cycle of F_{CO2}. Comparing our full seasonal uptake estimates to those calculated from average published F_{CO2} values extrapolated over 100 days results in seasonal CO_2 uptake under- or overestimates of 3.4 and 21 Tg C, respectively (Table 6). However,

we note that differences in the calculation of F_{CO2} would result in differences between our seasonal uptake estimates and those of other studies. For example, the use of the wind speed parameterization of Wanninkof et al. (1992) results in an overall average F_{CO2} that is -0.19 mmol m^{-2} d^{-1} smaller than our F_{CO2} using Ho et al. (2006).

We note that our method for calculating total seasonal CO_2 uptake is subject to several relevant uncertainties. First, our use of wind speeds from Pt. Barrow, AK probably do not necessarily represent those of the entire Chukchi shelf. However, these are currently the best estimate given that shipboard wind speeds are not yet available. Furthermore, our linear interpolation between observational time periods is subject to uncertainties due to the fact that changes to temperature, salinity, primary productivity, and ice concentrations are not strictly known due to the lack of observational data. Our results further demonstrate the importance of the use of different wind speeds, which would result in different seasonal CO_2 uptake estimates of up to three orders of magnitude (Table 5). Our study is the first of its kind to include observations from early spring into fall to estimate CO_2 uptake. While our calculation of air-sea CO_2 fluxes within and between seasons suffers from some inherent uncertainties, we suggest that the consideration of multiple observations reduces some of the uncertainty from extrapolating based on one set of observations from one season.

Summary

We report the first description of the changes to the inorganic carbon system during spring, summer and fall from within one ice melt and phytoplankton growing season in the western Arctic Ocean. Our results suggest that the later onset of sea ice

retreat had an important influence on the duration of the phytoplankton growing season in both the Chukchi Sea and Canada Basin. The reduced transmission of light through sea ice in June may have prevented the occurrence of the under ice blooms described by Arrigo et al. (2012), and could have instead resulted in a dominance of biological productivity following the ice edge. Areas exposed to longer ice-free conditions (i.e S. Chukchi Sea) exhibited earlier biological uptake and subsequent addition of CO_2 than areas where ice retreat had only recently occurred. The distribution of biologically-related pCO_2 values in earlier ice retreat years (i.e 2008 and 2012) compared to 2014 lends support to this conclusion.

We also report total CO_2 uptake estimates for the Chukchi shelf in 2014 based on a dataset spanning several important time periods in the ice retreat and phytoplankton growing season. These estimates are in the range of those previously published, but are potentially more accurate given their temporal coverage. Our results demonstrate the importance of the timing of observational studies in the Arctic Ocean, and could help improve the planning of future research expeditions. Given the observational gaps for the carbonate system of the Arctic Ocean in late summer and the potential for late season storms to cause outgassing of subsurface CO_2 and/or secondary phytoplankton blooms, we suggest that future research expeditions target late fall observational periods.

TABLES

Table 1) Summary of measured carbonate and associated parameters during the SUBICE spring 2014 cruise. See text for geographical and temporal definitions. ML = Mixed Layer; SS = Subsurface.

Spatial Definition	Temp. (°C)	Salinity (PSU)	Ice Conc. (%)	*n*DIC (µmol/kg^{-1})	*n*TA (µmol/kg^{-1})	pCO_2 (µatm)	ΔDIC (µmol/kg^{-1})
S. Chukchi	-1 ± 0.3	31.9 ± 0.3	24.6 ± 25.2	2092.4 ± 38.2	2232.7 ± 14.5	306.1 ± 84.5	-75.7 ± 32.9
1 - 51 m	-1.5 to -0.4	31.3 - 32.2	0 - 50.4	2010.6 - 2216.3	2208.9 - 2269.8	178.9 - 586	-157.2 to 14.4
	20	20	20	20	20	20	20
Beaufort ML	-1.6 ± 0	30.6 ± 0.1	99.3 ± 0.9	2133.2 ± 14.3	2241 ± 11.2	359.6 ± 29.5	-33.6 ± 9.9
2 - 25 m	-1.6 to -1.6	30.4 - 30.9	98 - 100	2115.2 - 2168.3	2226.4 - 2265.3	326.8 - 403.8	-45.9 to -17
	12	12	12	11	11	11	11
Beaufort SS	-1.6 ± 0	32 ± 0.4	99.4 ± 0.9	2188.4 ± 15.9	2250.6 ± 6.8	529.5 ± 79.3	7 ± 16.4
50 - 120 m	-1.7 to -1.6	31 - 32.3	98 - 100	2170.2 - 2209.5	2244.1 - 2264.2	432.2 - 638.2	-15 to 28
	7	7	7	7	7	7	7
Early ML	-1.7 ± 0	32.2 ± 0.3	95.1 ± 5.2	2207.1 ± 20.5	2255.1 ± 16	607.4 ± 129.8	24.5 ± 20.8
2 - 50 m	-1.7 to -1.6	31.5 - 32.8	78 - 100	2097.1 - 2291.9	2214 - 2308.5	242.1 - 1334	-74.7 to 102.5
	122	122	122	110	110	110	83
Early SS	-1.8 ± 0	32.6 ± 0.3	94.6 ± 5.2	2214.5 ± 20.7	2254.9 ± 8.9	645.9 ± 106	26.6 ± 23.1
21 - 72 m	-1.8 to -1.7	32 - 33	78 - 100	2137 - 2249.1	2240.6 - 2278.9	374.6 - 835.8	-45.3 to 45.3
	31	31	31	30	30	30	15
Late ML	-1.5 ± 0.3	32.2 ± 0.4	91.6 ± 13.8	2173.4 ± 43.3	2252.5 ± 20	485.6 ± 136.5	-15.8 ± 34.5
2 - 50 m	-1.7 to 0.4	29.9 - 32.7	30.4 - 100	2054.1 - 2227.9	2176.2 - 2285.9	223.9 - 1092.1	-101.5 to 23.7
	62	62	62	55	55	55	51
Late SS	-1.7 ± 0	32.5 ± 0.2	90.1 ± 14.1	2200.1 ± 18.1	2257.8 ± 9.9	556.3 ± 83.4	10 ± 15.4
5 - 58 m	-1.7 to -1.5	31.6 - 32.8	51.2 - 100	2164.1 - 2230.8	2237.7 - 2282.3	414.4 - 765.3	-11.5 to 42
	42	42	42	32	32	32	12

Note: values are reported as mean ± SD, range, and n.

Table 1) Continued

Spatial Definition	SiO_4^- (µmol/kg^{-1})	NO_3^- (µmol/kg^{-1})	PO_4^- (µmol/kg^{-1})	DO (µmol/kg^{-1})	AOU (µmol/kg^{-1})	Chl *a* (mg m^{-3})
S. Chukchi	23.7 ± 11.9	7.2 ± 4.9	1.1 ± 0.3	391.1 ± 15.3	-25.2 ± 17	4.2 ± 3
1 - 51 m	6.3 - 39	0 - 14	0.6 - 1.7	363 - 413.6	-50.5 to 4.6	0.5 - 9.2
	20	18	20	20	20	15
Beaufort ML	8.1 ± 2.7	1.6 ± 1	0.8 ± 0	385.7 ± 8.4	-9.8 ± 8	0.8 ± 0.3
2 - 25 m	6.3 - 15.7	1 - 4.5	0.7 - 1	359.3 - 389.6	-13.2 to 15.3	0.2 - 1.5
	12	12	12	12	12	12
Beaufort SS	29.5 ± 7.7	8.5 ± 1.6	1.4 ± 0.2	329 ± 18	43.2 ± 16.9	0.1 ± 0
50 - 120 m	16.4 - 37.7	5.3 - 10	1.1 - 1.6	313.3 - 367.6	6.8 to 57.9	0 - 0.2
	7	7	7	7	7	7
Early ML	44.4 ± 7.7	11.6 ± 2.4	1.7 ± 0.2	329.1 ± 16.9	42.8 ± 17.3	0.8 ± 1.6
2 - 50 m	0 - 52.5	3 - 15.5	0 - 1.9	304.5 - 392.1	-20.5 to 68.2	0.1 - 9.5
	117	115	117	122	122	120
Early SS	47.9 ± 5.9	12.8 ± 2.6	1.9 ± 0.1	317.9 ± 19.5	53.5 ± 19.6	0.5 ± 1.3
21 - 72 m	32.8 - 57.4	6.3 - 16.3	1.4 - 2.2	283.8 - 364.5	6.6 to 88	0 - 6.8
	31	31	31	31	31	31
Late ML	42.4 ± 12	11.5 ± 3.6	1.6 ± 0.3	362 ± 37.9	8.5 ± 38.5	3.1 ± 2.2
2 - 50 m	6.2 - 52.5	0 - 15.3	0.6 - 1.9	307.4 - 463.6	-93.1 to 64.7	0.3 - 8.9
	56	54	56	62	62	64
Late SS	48.9 ± 6.9	13.8 ± 2.1	1.9 ± 0.2	334.4 ± 33.4	36.6 ± 33.2	3.1 ± 3
5 - 58 m	32.4 - 61.8	8.2 - 16.9	1.4 - 2.3	285.9 - 429.3	-58.7 to 85.6	0.3 - 11.9
	33	33	33	42	42	42

Note: values are reported as mean ± SD, range, and n.

Table 2 Summary of measured carbonate and associated parameters during the CHINARE summer 2014 cruise on the Chukchi shelf. See text for geographical and temporal definitions. ML = Mixed Layer; SS = Subsurface; UHL = Upper Halocline Layer; LHL = Lower Halocline Layer; (Ice free) refers to ice-free shelf stations, while (Ice) refers to intermediate ice cover shelf stations

Spatial Definition	Temp. (°C)	Salinity (PSU)	Ice Conc. (%)	*n*DIC (µmol/kg^{-1})	*n*TA (µmol/kg^{-1})	pCO_2 (µatm)	ΔDIC (µmol/kg^{-1})
Shelf ML (Ice Free)	5.4 ± 2.3	31 ± 1	0 ± 0	1985.8 ± 54.2	2232.7 ± 21.9	217.4 ± 66.9	-162 ± 54.9
3 - 11 m	-1.3 to 9.3	28.4 - 32.6	0 - 0	1852 - 2052.5	2195.3 - 2268.5	112.3 - 355.7	-293.1 to -90.4
	24	24	24	24	24	24	23
Shelf SS (Ice Free)	2.8 ± 2.6	31.8 ± 0.6		2039 ± 66.9	2238.6 ± 19.4	256.1 ± 92.6	-131.3 ± 52.9
10 - 59 m	-1.6 to 9	29.3 - 32.8		1847.6 - 2249.5	2198 - 2288.1	108.1 - 655.2	-296.6 to 27.8
	60	60		59	59	59	51
Shelf ML (Ice)	-1.1 ± 0.2	28.5 ± 1.3	43 ± 17.4	1984.7 ± 41.9	2190.3 ± 37	194.7 ± 59.2	-113 ± 56.1
3 - 5 m	-1.3 to -0.6	27.1 - 30.3	18 - 57.6	1939.5 - 2034.2	2126 - 2221.1	124.1 - 273.2	-190.1 to -45.8
	6	6	6	6	6	6	6
Shelf SS (Ice)	-1.4 ± 0.1	31.3 ± 0.9		2148 ± 45.2	2256.9 ± 17	381.5 ± 117.3	-34.9 ± 32.2
10 - 58 m	-1.7 to -1.1	28.1 - 32.8		2078 - 2253.1	2220 - 2282.5	239.2 - 696.9	-94 to 8.1
	22	22		19	19	19	21
Shelf UH (Ice)	-1.6 ± 0.1	32.6 ± 0.1		2275.1 ± 11.2	2215.2 ± 23.6	545 ± 73.5	-4.7 ± 7.2
66 - 101	-1.7 to -1.3	32.4 - 32.9		2258.8 - 2293.5	2193.5 - 2252.7	470.8 - 635.3	-10.5 to 3.4
	6	6		6	6	6	3
Shelf LH (Ice)	-0.7 ± 0.8	33.7 ± 0.7		2175.9 ± 36.7	2271.7 ± 12.4	440.3 ± 102.4	ND
127 - 183 m	-1.4 to 0.2	33.1 - 34.6		2143.7 - 2217.6	2261.7 - 2293.3	364 - 597.9	ND
	7	7		5	5	5	ND

Note: values are reported as mean ± SD, range, and n.

Table 2) Continued

Spatial Definition	SiO_4^- (µmol/kg^{-1})	NO_3^- (µmol/kg^{-1})	PO_4^- (µmol/kg^{-1})	DO (µmol/kg^{-1})	AOU (µmol/kg^{-1})	Chl *a* (mg m^{-3})
Shelf ML (Ice Free) 3 - 11 m	4.1 ± 3.2 0.2 - 12 24	0.2 ± 0.1 0 - 0.8 24	0.4 ± 0.1 0.2 - 0.6 24	345.1 ± 61.8 245.6 - 482 21	-29 ± 54.2 -110.4 to 70.9 21	1 ± 1.1 0.2 - 5.3 20
Shelf SS (Ice Free) 10 - 59 m	8.5 ± 7.9 1.3 - 46 45	2.8 ± 4.2 0.1 - 14 45	0.8 ± 0.3 0.4 - 1.7 45	325.8 ± 45.1 198.9 - 422.5 59	6.9 ± 46.9 -86.8 to 129.9 59	2.1 ± 3.1 0.3 - 18.8 47
Shelf ML (Ice) 3 - 5 m	7.7 ± 4.2 3.1 - 12.9 6	0.2 ± 0.1 0.1 - 0.4 6	0.6 ± 0 0.6 - 0.7 6	447.3 ± 49.8 397.9 - 512.9 5	-70.5 ± 53.2 -140.2 to -17.4 5	1.4 ± 2 0 - 5.4 6
Shelf SS (Ice) 10 - 58 m	25 ± 14.3 5.2 - 59.6 17	8.3 ± 6.2 0.2 - 22 17	1.3 ± 0.3 0.7 - 2.1 17	365.6 ± 45.4 269.3 - 422.4 18	6.1 ± 44.7 -50.4 to 101.1 18	3.2 ± 3.6 0.1 - 11.5 22
Shelf UHL (Ice) 66 - 101	40.4 ± 12 26.7 - 59.8 6	16.8 ± 3.1 13.8 - 22.1 6	1.8 ± 0.2 1.5 - 2.2 6	313.1 ± 26.7 267.9 - 344.3 6	56.7 ± 27.3 23.2 to 102.3 6	0.4 ± 0.5 0 - 1.6 6
Shelf LHL (Ice) 127 - 183 m	21.2 ± 10 15.3 - 32.7 3	16.4 ± 0.7 15.6 - 16.9 3	1.2 ± 0.3 1 - 1.6 3	277.4 ± 14.9 261.3 - 296.5 5	78.3 ± 7.1 70 to 84.8 5	0.2 ± 0.1 0 - 0.4 5

Note: values are reported as mean ± SD, range, and n.

Table 3 Summary of measured carbonate and associated parameters during the CHINARE summer 2014 cruise in the Canada Basin. See text for geographical and temporal definitions. C Basin = Canada Basin; ML = Mixed Layer; SS = Subsurface; UHL = Upper Halocline Layer; LHL = Lower Halocline Layer

Spatial Definition	**Temp. (°C)**	**Salinity (PSU)**	**Ice Conc. (%)**	***n*DIC (µmol/kg^{-1})**	***n*TA (µmol/kg^{-1})**	***p*CO$_2$ (µatm)**	**ΔDIC (µmol/kg^{-1})**
C Basin ML	-1.1 ± 0.1	27.5 ± 0.5	62.2 ± 31.3	2010.9 ± 32.3	2141.1 ± 36.8	290 ± 26.7	-41.3 ± 13.7
3 - 5 m	-1.4 to -0.6	26.7 - 28.7	0 - 100	1947.6 - 2064.3	2088.1 - 2211.7	240.6 - 330.5	-70.9 to -21.8
	20	20	20	20	20	20	20
C Basin PSW	-0.8 ± 0.4	29.9 ± 1.2		2085.2 ± 28.4	2226.2 ± 36.4	291.5 ± 30.8	-60.5 ± 20.5
5 - 58 m	-1.3 to 0.1	27.1 - 31.6		2002.8 - 2136.5	2099.5 - 2278.5	226 - 360.2	-107.3 to 0
	50	50		49	49	49	50
C Basin UH	-1 ± 0.2	32 ± 0.3		2162.3 ± 20.6	2258.5 ± 14.5	416.7 ± 67.2	-26.9 ± 20.6
61 - 125 m	-1.5 to -0.2	30.7 - 32.6		2112.1 - 2201.4	2233.8 - 2283.5	262 - 597.9	-82.5 to 4.4
	43	43		42	42	42	42
C Basin LH	-1.3 ± 0.1	33.1 ± 0.4		2211 ± 18.2	2272.5 ± 14.8	552 ± 84.9	-8.3 ± 26.1
149 - 200	-1.6 to -0.8	32.5 - 34.1		2157.9 - 2237.8	2248.4 - 2301.9	372.2 - 722	-26.8 to 10.1
	43	43		43	43	43	2

Note: values are reported as mean ± SD, range, and n.

Table 3) Continued

Spatial Definition	SiO_4^- (µmol/kg^{-1})	NO_3^- (µmol/kg^{-1})	PO_4^- (µmol/kg^{-1})	DO (µmol/kg^{-1})	AOU (µmol/kg^{-1})	Chl *a* (mg m^{-3})
C Basin ML	2.9 ± 0.3	0.1 ± 0.1	0.6 ± 0	395.3 ± 14.1	-15.4 ± 13.5	0 ± 0
3 - 5 m	2.4 - 3.8	0 - 0.3	0.5 - 0.7	360.3 - 409	-33.2 to 17.8	0 - 0.1
	19	19	19	15	15	10
C Basin PSW	5 ± 2.5	0.8 ± 1.2	0.8 ± 0.1	390 ± 19.7	-20.6 ± 16.7	0.3 ± 0.3
5 - 58 m	2.5 - 11.4	0 - 4.4	0.5 - 1.1	333 - 413.9	-42.3 to 29	0 - 1.7
	46	46	46	42	42	23
C Basin UH	18.9 ± 5.4	8.9 ± 3	1.4 ± 0.2	326.1 ± 18.6	39.9 ± 19.4	0.1 ± 0.1
61 - 125 m	6.8 - 29.2	0.6 - 13	0.8 - 1.7	276.3 - 371.7	-9.9 to 89.4	0 - 0.4
	37	37	37	40	40	18
C Basin LH	31 ± 4.5	14.9 ± 1.1	1.8 ± 0.1	287.7 ± 10.6	78.3 ± 9.5	0 ± 0
149 - 200	17.2 - 37.2	11.5 - 16.6	1.1 - 2	267.1 - 329.1	41.6 to 99	0 - 0
	30	30	30	41	41	18

Note: values are reported as mean ± SD, range, and n.

Table 4) Summary of measured carbonate and associated parameters during the MR 2014 fall cruise. See text for geographical and temporal definitions.
ML = Mixed Layer; SS = Subsurface; UH = Upper Halocline; Nutrient data unavailable. All ice concentrations = 0%.

	Temp. (°C)	**Salinity (PSU)**	***n*DIC (µmol/kg^{-1})**	***n*TA (µmol/kg^{-1})**
S. Chukchi ML	4.6 ± 1.8	32 ± 0.3	2012.2 ± 69.4	2222.3 ± 11.5
3 - 10 m	2.7 to 6.9	31.5 - 32.3	1927.3 - 2090.2	2209.8 - 2236.7
(3-Sept.)	6	6	6	6
S. Chukchi SS	2.7 ± 0.9	32.4 ± 0.2	2148.8 ± 56.9	2228.9 ± 8
10 - 53 m	1.9 to 5.6	31.8 - 32.8	2039.2 - 2213.8	2219.9 - 2241.7
(3-Sept.)	16	16	16	16
S. Chukchi ML	5.6 ± 1.2	31.7 ± 0.2	2221.1 ± 12.1	2036.8 ± 31.5
5 - 50 m	4.6 to 7	31.5 - 31.9	2206.1 - 2233.9	1997.3 - 2064.2
(28-Sept.)	5	5	5	5
S. Chukchi SS	3.1 ± 0.3	32.3 ± 0.4	2127.8 ± 44.9	2229.1 ± 12.8
15 - 50 m	2.9 to 3.8	31.9 - 32.9	2096.2 - 2219.4	2214.3 - 2247
(28-Sept.)	11	11	11	11
Chukchi ML	2.8 ± 1.1	30.6 ± 1.1	2002.2 ± 26.3	2187.5 ± 38.4
4 - 29 m	0 to 5	25.7 - 31.3	1899.4 - 2034.2	2030 - 2223.6
	36	36	36	36
Chukchi SS	0.7 ± 1.8	31.3 ± 1.3	2089.3 ± 81.4	2216.3 ± 39.7
9 - 50 m	-1.6 to 4.6	25.9 - 32.6	1902.6 - 2200.1	2078.9 - 2254.3
	56	56	56	56
Chukchi UHL	-1.2 ± 0.5	32.7 ± 0.4	2221.9 ± 22.8	2250 ± 10.2
50 - 100 m	-1.7 to -0.4	32.3 - 33.9	2183.7 - 2260.8	2233 - 2270.6
	12	12	12	12

Table 4) Continued

	pCO_2 (µatm)	ΔDIC (µmol/kg^{-1})	DO (µmol/kg^{-1})	AOU (µmol/kg^{-1})	Chl *a* (mg m^{-3})
S. Chukchi ML	255.9 ± 77	-150 ± 52.3	344.7 ± 8.9	-27.5 ± 15.1	16.3 ± 10.3
3 - 10 m	176.9 - 374.5	-209.9 to -82.5	332.8 - 355.6	-38.3 to -1.5	3.7 - 28
(3-Sept.)	6	6	6	6	6
S. Chukchi SS	592.6 ± 192.5	-49.1 ± 48.8	273.4 ± 44.7	57.3 ± 50	8 ± 10.5
10 - 53 m	254.8 - 856.3	-141.4 to -9.9	218.9 - 349	-28.7 to 111.5	0.7 - 31.9
(3-Sept.)	16	12	16	16	14
S. Chukchi ML	294.4 ± 21.5	-111.9 ± 20.6	317 ± 10.4	-6.4 ± 2.4	4.9 ± 3.1
5 - 50 m	266.5 - 311.4	-95.4 to -138.9	305.5 - 325.2	-8.8 to -3.4	1.3 - 6.7
(28-Sept.)	5	5.0	5	5	3
S. Chukchi SS	500.2 ± 202.3	-62 ± 10.8	278.8 ± 37.1	48.7 ± 38.4	2.2 ± 0.7
15 - 50 m	368.6 - 925.9	-85.6 to -55.6	204.9 - 315	8 to 123.2	1.3 - 3.8
(28-Sept.)	11	7	11	11	9
Chukchi ML	250.4 ± 19.3	-104.2 ± 19.2	338.7 ± 11.5	-3.6 ± 1.8	0.9 ± 1.7
4 - 29 m	226.4 - 309.6	-118 to -32	321.4 - 368.4	-8.3 to 0.4	0.3 - 8.7
	36	36	36	36	22
Chukchi SS	373.1 ± 135.3	-56.5 ± 47.6	343.6 ± 47.4	7.9 ± 45.5	0.6 ± 0.9
9 - 50 m	178.4 - 626	-180.2 to 21.2	271.5 - 454.8	-107.3 to 87.2	0 - 6.1
	56	54	56	56	46
Chukchi UHL	719 ± 130.1	26.4 ± 18.1	275 ± 26.6	91.1 ± 24	0.1 ± 0.1
50 - 100 m	564.9 - 967.5	2.8 to 45.6	220.7 - 309.9	60.2 to 138.6	0 - 0.4
	12	7	12	12	12

Table 5) Calculated air-sea CO2 fluxes (mmol m^{-2} d^{-1}) for May - Dec. 2014. See main text for descriptions of study periods and methodologies used.

Wind Speed	**15 May - 3 Jun.**	**4 - 19 Jun.**	**19 Jun. - 27 Jul.**	**27 Jul. - 7 Aug.**
Daily	-0.35 ± 2.7 -11.2 to 2.89	-0.5 ± 1.72 -5.7 to 0.6	-3.7 ± 5.2 -16.9 to 1.2	-11.9 ± 10.7 -42.7 to -1.7
Seasonal	0.08 ± 2.6 -9.0 to 4.39	-0.62 ± 2.4 -7.9 to 1.9	-3.7 ± 4.7 -14.1 to 0.8	-13.7 ± 5.7 -23.4 to -2.9
Seasonal Min.	0.0006 ± 0.02 -0.07 to 0.03	-0.005 ± 0.02 -0.06 to 0.014	-0.03 ± 0.03 -0.1 to 0.01	-0.1 ± 0.04 -0.17 to -0.02
Seasonal Max.	0.478 ± 15.06 -52.1 to 25.3	-3.584 ± 14.04 -45.7 to 11.0	-22.4 ± 27.9 -84.2 to 4.9	-78.74 ± 33.08 -134.8 to -16.9

Table 5) continued

Wind Speed	7 Aug. - 3 Sept.	3 - 28 Sept.	28 Sept. - 15 Dec.	Seasonal Average	Total CO_2 uptake (Tg C)
Daily	-19.7 ± 15.5 -59.7 to -2.0	-15.3 ± 10.3 -37.2 to -1.8	-2.7 ± 6.3 -21.1 to 11.3	-7.74	10.2
Seasonal	-13.0 ± 0.7 -14.1 to -11.7	-11.1 ± 3.9 -18.0 to -1.3	-1.7 ± 4.3 -12.6 to 2.2	-6.25	7.7
Seasonal Min.	-0.95 ± 0.05 -0.1 to -0.09	-0.082 ± 0.03 -0.13 to -0.01	-0.01 ± 0.03 -0.09 to 0.02	-0.17	0.08
Seasonal Max.	-77.4 ± 4.4 -84.2 to -69.9	-63.96 ± 22.43 -103.9 to -7.49	-9.5 ± 23.9 -69.9 to 11.9	-36.44	44.7

Table 6 Average air-sea CO2 flux rates and total seasonal CO2 uptake estimates on the Chukchi Shelf (595,000 km2)

Reference	**Air-sea Flux (mmol m^{-2} d^{-1})**	**CO_2 uptake (g C yr^{-1})**
Pipko et al. (2002)	-14.6	10.4
Murata & Takizawa (2003)	-12	8.6
Bates (2006)	-40	28.6
Semilitov et al. (2007)	-11.9	8.5
Gao et al. (2012)	-17	12.1
Evans et al. (2015)	-6	4.3
This study	-6.25	7.7*
*Note: our CO_2 uptake uses calculated F_{CO2} in spring, summer, and fall with linearly interpolated F_{CO2} between observations.		

FIGURES

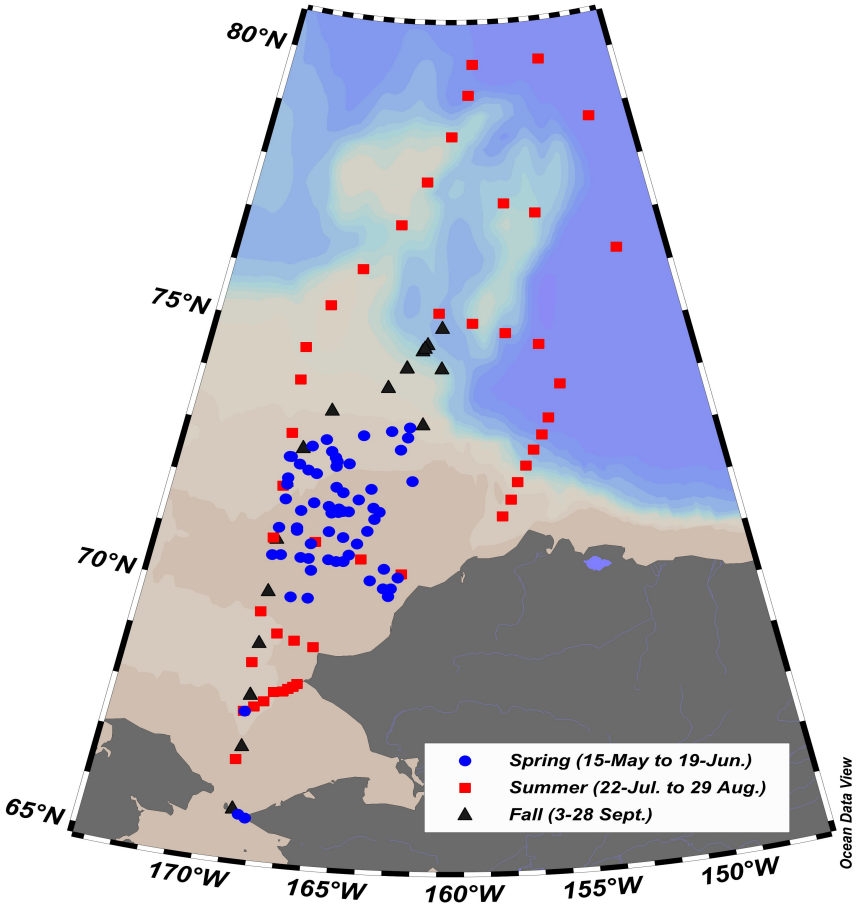

Figure 1) Station locations for spring, summer and fall hydrographic stations in 2014.

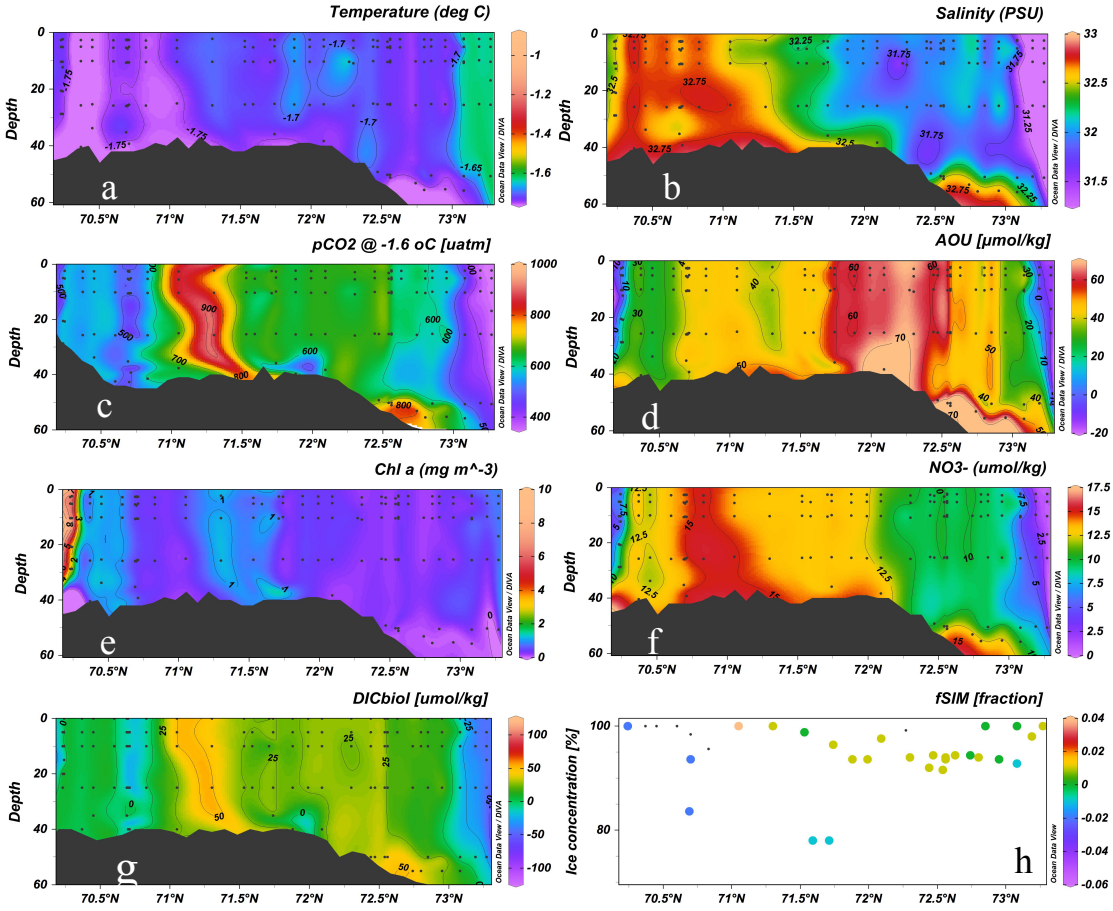

Figure 2) Distribution of physical and biogeochemical parameters on the Chukchi shelf in early spring. Note that DICbiol = ΔDIC in the main text.

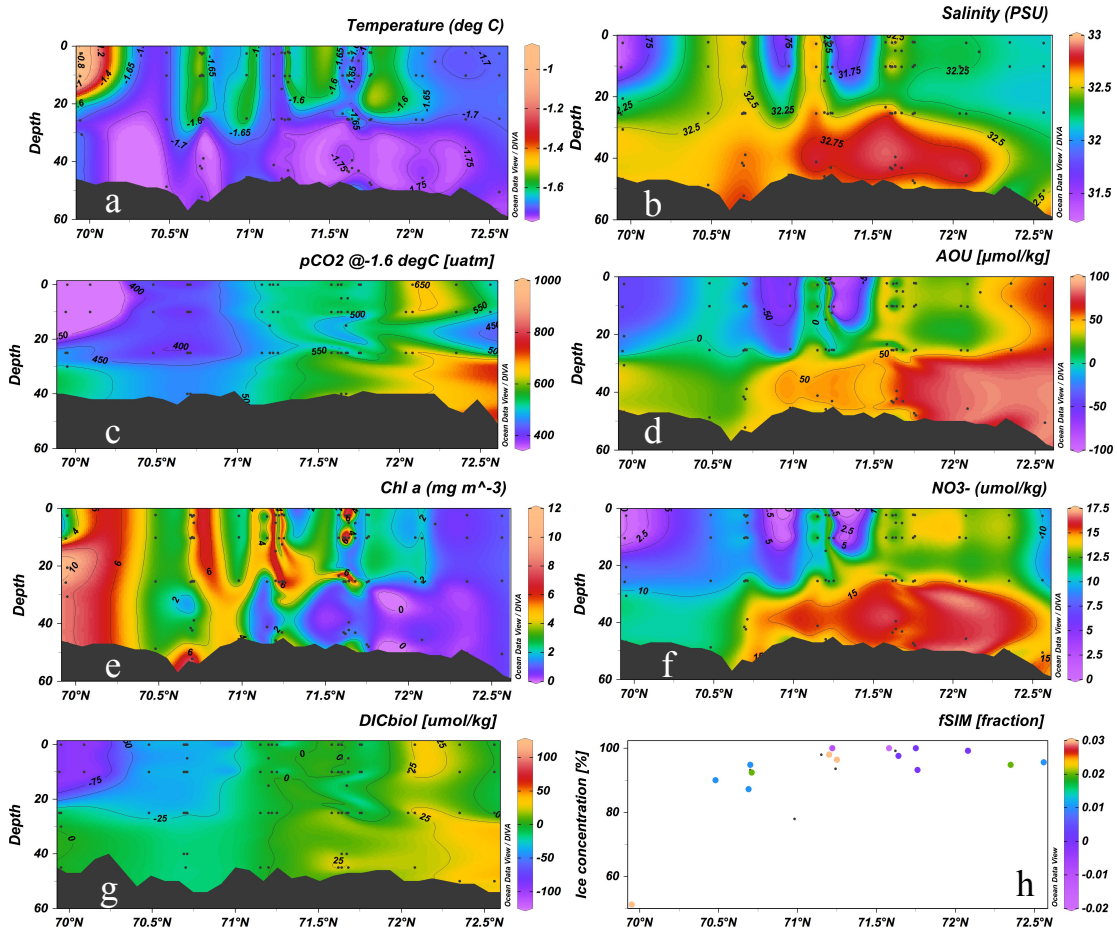

Figure 3) Distribution of physical and biogeochemical parameters on the Chukchi shelf in late spring. Note that DICbiol = ΔDIC in the main text.

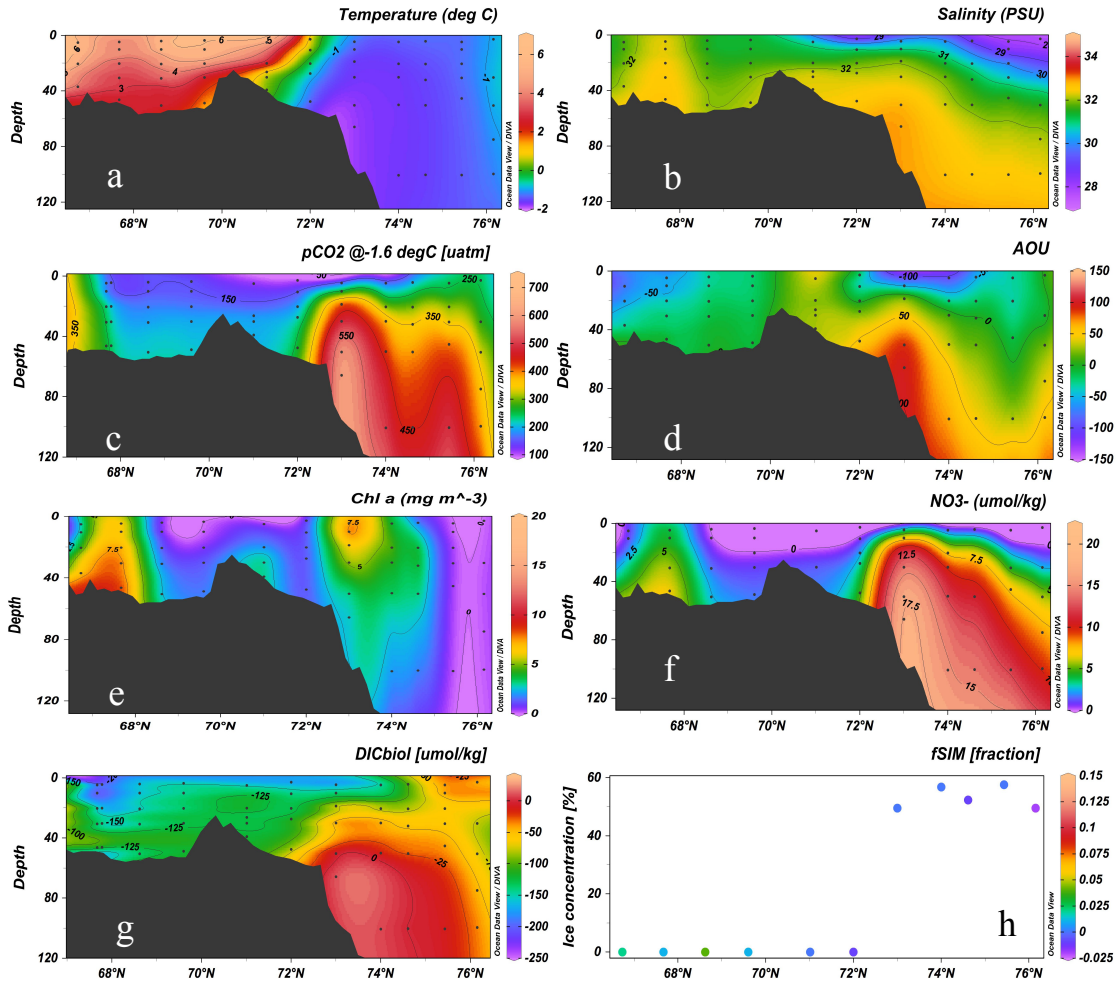

Figure 4) Distribution of physical and biogeochemical parameters on the Chukchi shelf in summer. Note that DICbiol = ΔDIC in the main text.

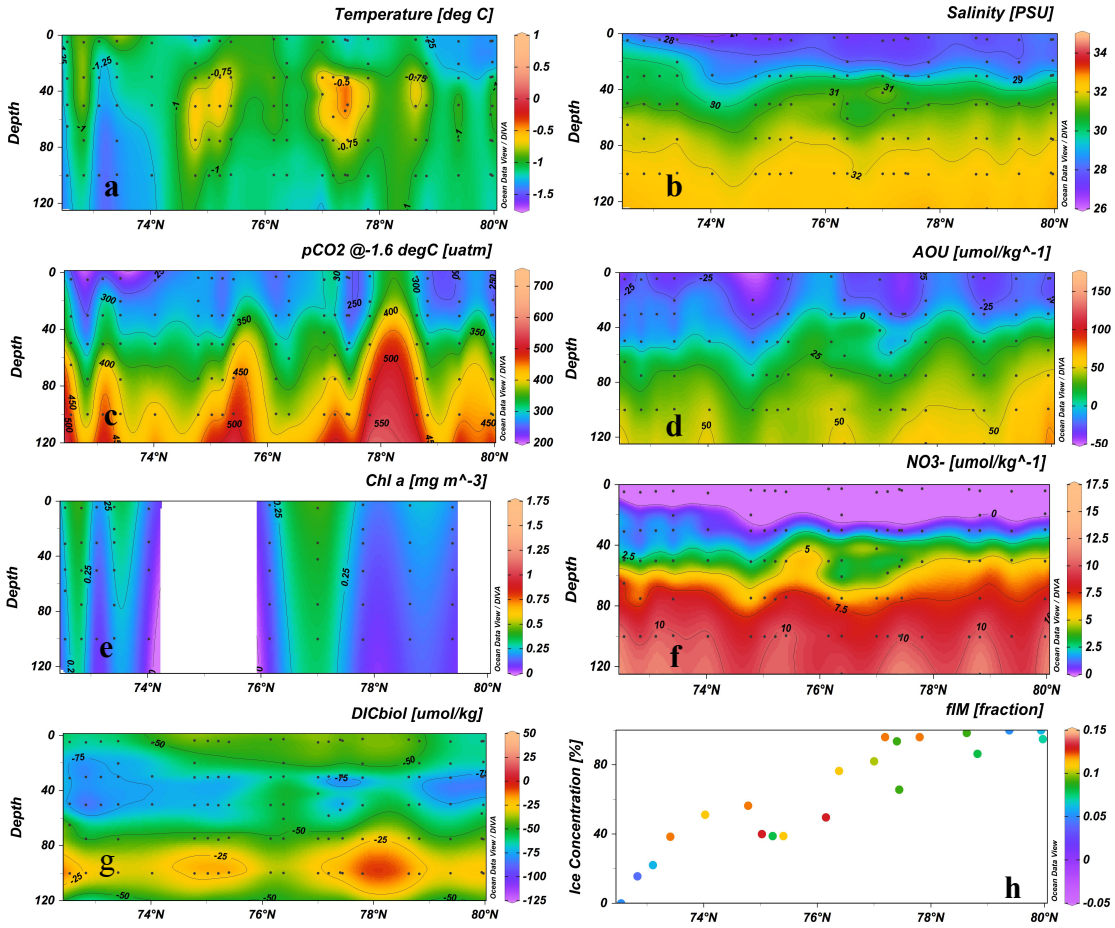

Figure 5) Distribution of physical and biogeochemical parameters in the Canadian Basin in summer. Note that DICbiol = ΔDIC in the main text.

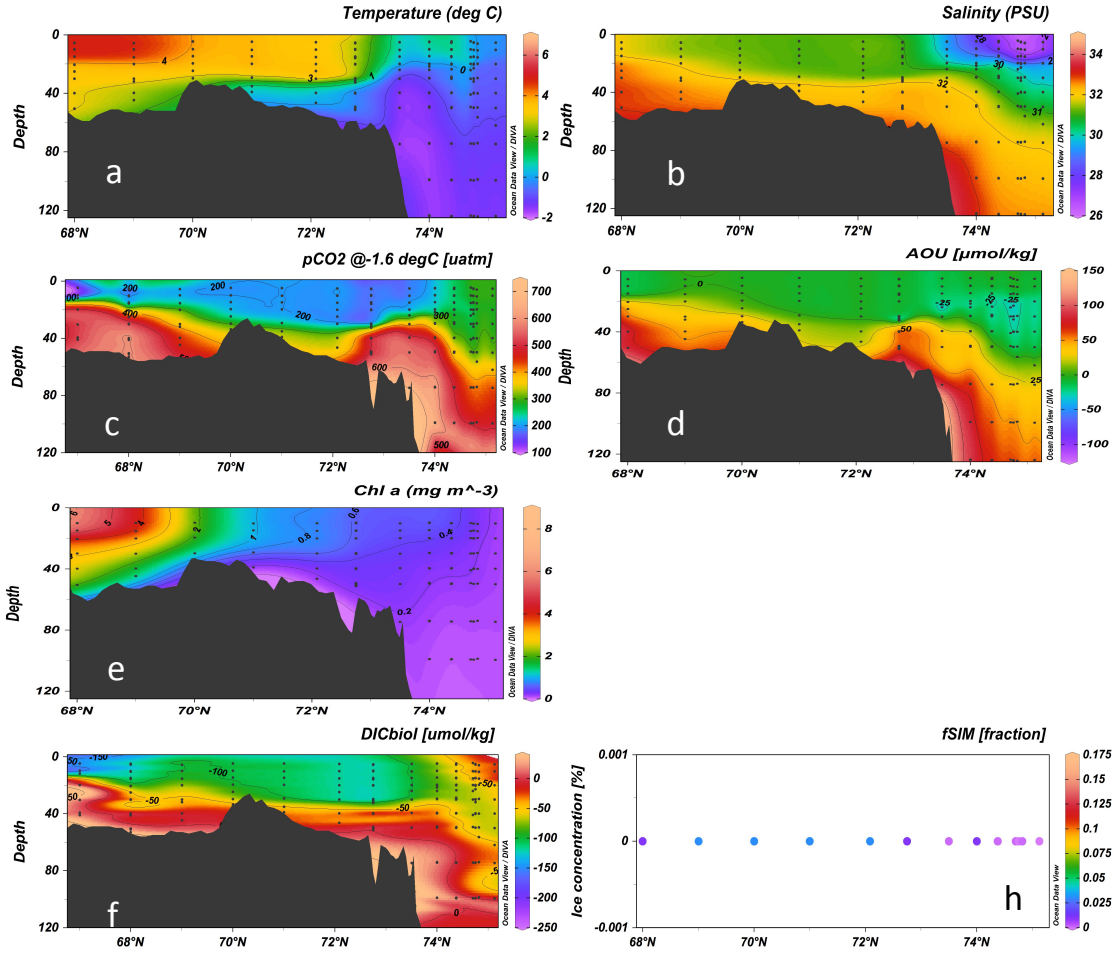

Figure 6) Distribution of physical and biogeochemical parameters in Chukchi Sea in fall. Note that DICbiol = ΔDIC in the main text. NO_3^- is absent due to data not being available yet.

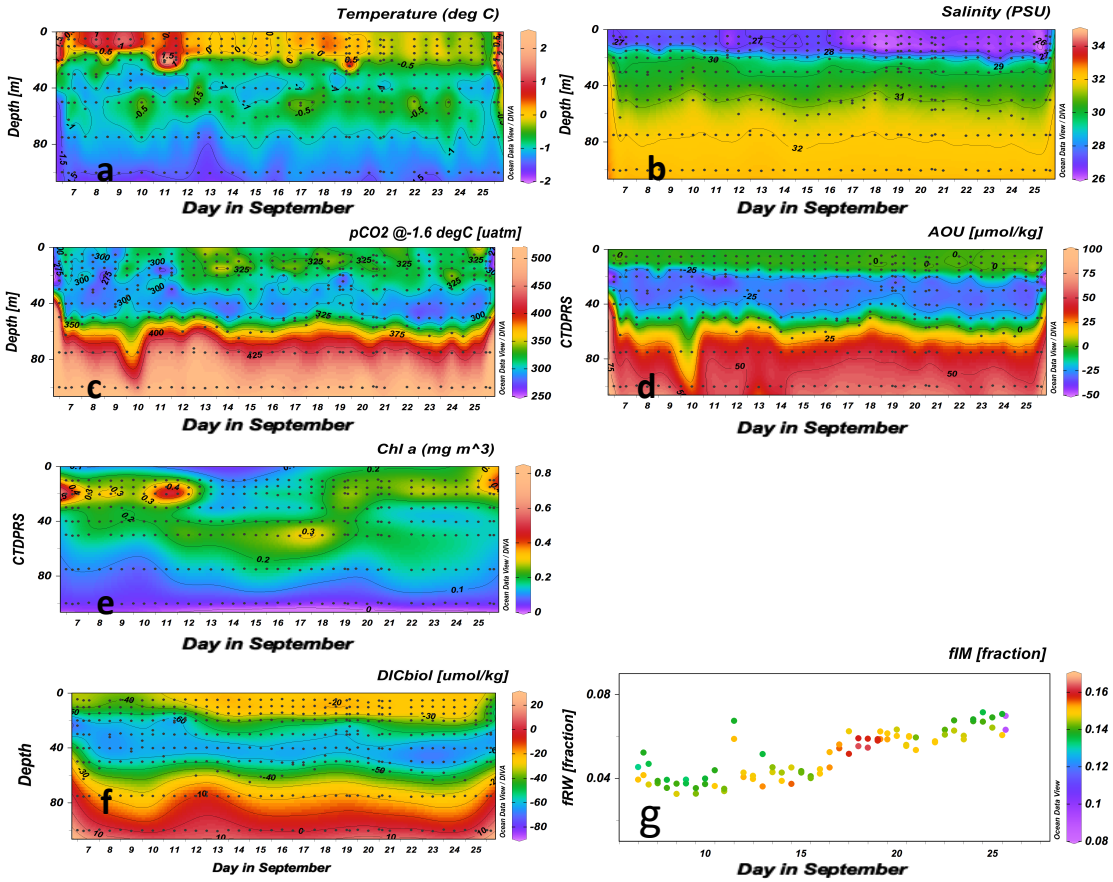

Figure 7) Distribution of physical and biogeochemical parameters in Chukchi Sea in fall at a fixed point observatory. Note that DICbiol = ΔDIC in the main text. NO_3^- is absent due to data not being available yet.

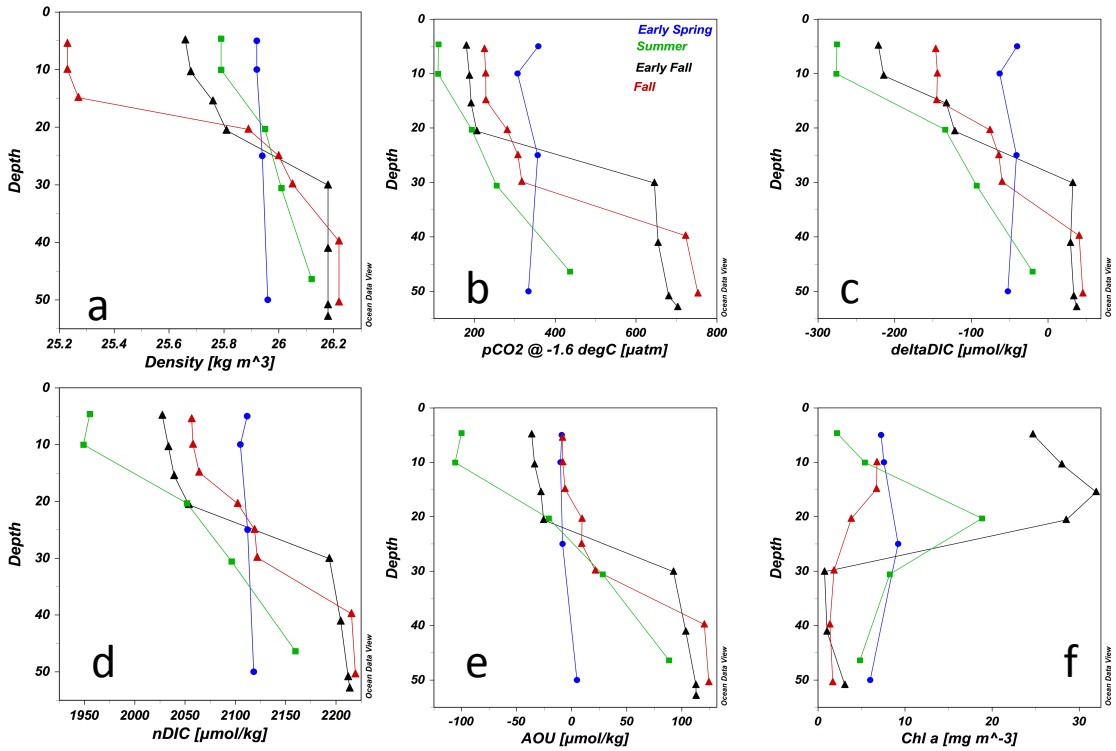

Figure 8) Physical and biogeochemical profiles of representative stations during spring, summer, and fall on the S. Chukchi shelf. Note that deltaDIC = ΔDIC in the main text. NO_3^- is absent due to data not being available yet. See plots for color descriptions of each time period.

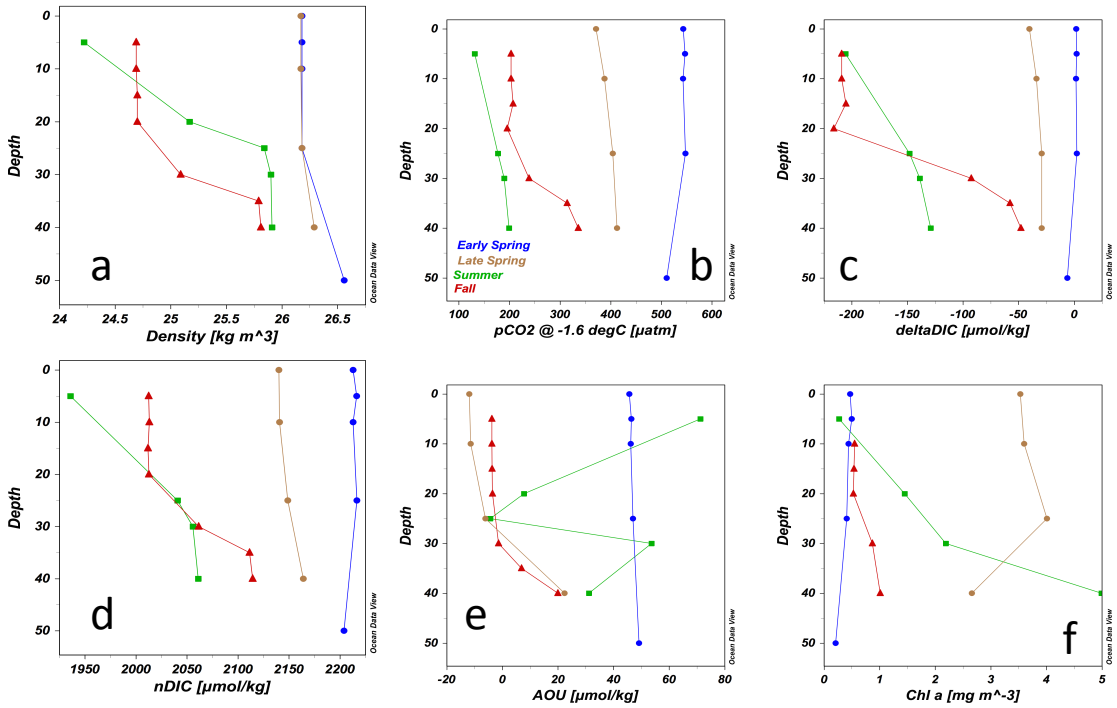

Figure 9) Physical and biogeochemical profiles of representative stations during spring, summer, and fall on the central Chukchi shelf. Note that deltaDIC = ΔDIC in the main text. NO_3^- is absent due to data not being available yet. See plots for color descriptions of each time period.

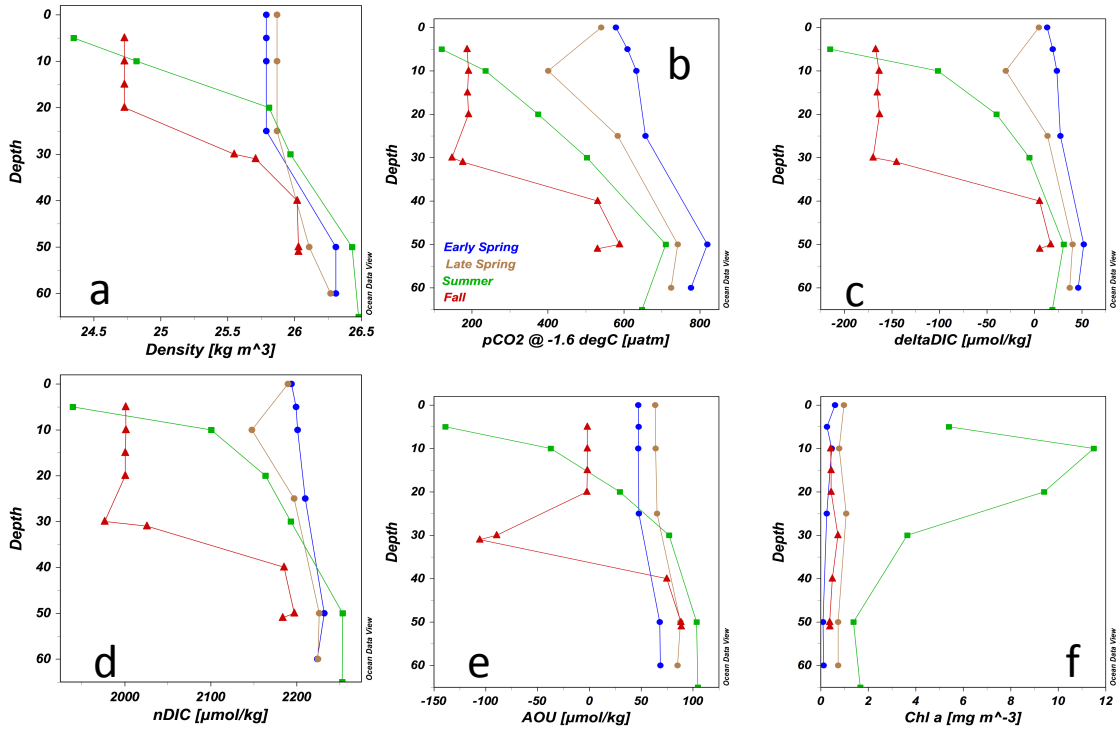

Figure 10) Physical and biogeochemical profiles of representative stations during spring, summer, and fall on the NE Chukchi shelf. Note that deltaDIC = ΔDIC in the main text. NO_3^- is absent due to data not being available yet. See plots for color descriptions of each time period.

REFERENCES

1. Aagaard, K., Swift, J. H., & Carmack, E. C. (1985). Thermohaline circulation in the Arctic Mediterranean Seas. *Journal of Geophysical Research*, *90*(C3), 4833. http://doi.org/10.1029/JC090iC03p04833
2. Ardyna, M., Babin, M., Gosselin, M., Devred, E., Rainville, L., & Tremblay, J.-éric. (2014). Fall Phytoplankton Blooms, 6207–6212. http://doi.org/10.1002/2014GL061047.
3. Armstrong, F. A. J., Stearns, C. R., & Strickland, J. D. H. (1967, June). The measurement of upwelling and subsequent biological process by means of the Technicon Autoanalyzer® and associated equipment. In *Deep Sea Research and Oceanographic Abstracts* (Vol. 14, No. 3, pp. 381-389). Elsevier.
4. Arrigo, K. R., van Dijken, G., & Pabi, S. (2008). Impact of a shrinking Arctic ice cover on marine primary production. *Geophysical Research Letters*, *35*(19), 1–6. http://doi.org/10.1029/2008GL035028
5. Arrigo, K. R., & Dijken, G. L. Van. (2011). Secular trends in Arctic Ocean net primary production. *Journal of Experimental Marine Biology and Ecology*, *116*(May), 1–15. http://doi.org/10.1029/2011JC007151
6. Arrigo, K. R., Perovich, D. K., Pickart, R. S., Brown, Z. W., Dijken, G. L. Van, Lowry, K. E., Swift, J. H. (2012). Under Arctic Sea Ice, *336*(June), 2012.
7. Arrigo, K. R., & van Dijken, G. L. (2015). Continued increases in Arctic Ocean primary production. *Progress in Oceanography*, *136*, 60–70. http://doi.org/10.1016/j.pocean.2015.05.002
8. Bates, N. R. (2006). Air-sea CO2 fluxes and the continental shelf pump of carbon in theChukchi Sea adjacent to the Arctic Ocean. *Journal of Geophysical Research: Oceans*, *111*(10), 1–21. http://doi.org/10.1029/2005JC003083

9. Bates, N. R., Mathis, J. T., & Cooper, L. W. (2009). Ocean acidification and biologically induced seasonality of carbonate mineral saturation states in the western Arctic Ocean. *Journal of Geophysical Research: Oceans*, *114*(11), 1–21. http://doi.org/10.1029/2008JC004862
10. Bates, N. R., Garley, R., Frey, K. E., Shake, K. L., & Mathis, J. T. (2014). Sea-ice melt CO_2-carbonate chemistry in the western Arctic Ocean: meltwater contributions to air-sea CO_2 gas exchange, mixed layer properties and rates of net community production under sea ice. *Biogeosciences Discussions*, *11*(1), 1097–1145. http://doi.org/10.5194/bgd-11-1097-2014
11. Brown, Z. W., Lowry, K. E., Palmer, M. a., van Dijken, G. L., Mills, M. M., Pickart, R. S., & Arrigo, K. R. (2015). Characterizing the subsurface chlorophyll a maximum in the Chukchi Sea and Canada Basin. *Deep Sea Research Part II: Topical Studies in Oceanography*, *118*, 1–17. http://doi.org/10.1016/j.dsr2.2015.02.010
12. Brugler, E. T., Pickart, R. S., Moore, G. W. K., Roberts, S., Weingartner, T. J., & Statscewich, H. (2014). Seasonal to interannual variability of the Pacific water boundary current in the Beaufort Sea. *Progress in Oceanography*, *127*, 1–20. http://doi.org/10.1016/j.pocean.2014.05.002
13. Cai, W.-J., Chen, L., Chen, B., Gao, Z., Lee, S. H., Chen, J., … Zhang, H. (2010). Decrease in the CO2 uptake capacity in an ice-free Arctic Ocean basin. *Science (New York, N.Y.)*, *329*(5991), 556–559. http://doi.org/10.1126/science.1189338
14. Carmack, E. (2003). Wind-driven shelf/basin exchange on an Arctic shelf: The joint roles of ice cover extent and shelf-break bathymetry. *Geophysical Research Letters*, *30*(14), 1778. http://doi.org/10.1029/2003GL017526
15. Carmack, E., & Wassmann, P. (2006). Food webs and physical-biological coupling on pan-Arctic shelves: Unifying concepts and comprehensive perspectives. *Progress in Oceanography*, *71*(2-4), 446–477. http://doi.org/10.1016/j.pocean.2006.10.004

16. Codispoti, L. a., Flagg, C. N., & Swift, J. H. (2009). Hydrographic conditions during the 2004 SBI process experiments. *Deep-Sea Research Part II: Topical Studies in Oceanography*, *56*, 1144–1163. http://doi.org/10.1016/j.dsr2.2008.10.013
17. Cooper, L. W., McClelland, J. W., Holmes, R. M., Raymond, P. a., Gibson, J. J., Guay, C. K., & Peterson, B. J. (2008). Flow-weighted values of runoff tracers (??18O, DOC, Ba, alkalinity) from the six largest Arctic rivers. *Geophysical Research Letters*, *35*(18), 3–7. http://doi.org/10.1029/2008GL035007
18. Coupel, P., Jin, H. Y., Joo, M., Horner, R., Bouvet, H. a., Sicre, M. a., … Ruiz-Pino, D. (2012). Phytoplankton distribution in unusually low sea ice cover over the Pacific Arctic. *Biogeosciences*, *9*(11), 4835–4850. http://doi.org/10.5194/bg-9-4835-2012
19. Else, B. G. T., Galley, R. J., Lansard, B., Barber, D. G., Brown, K., Miller, L. a., … Rysgaard, S. (2013). Further observations of a decreasing atmospheric CO2 uptake capacity in the Canada Basin (Arctic Ocean) due to sea ice loss. *Geophysical Research Letters*, *40*(6), 1132–1137. http://doi.org/10.1002/grl.50268
20. Evans, W., Mathis, J. T., Cross, J. N., Bates, N. R., Frey, K. E., Else, B. G. T., Takahashi, T. (2015). Sea-air CO_2 exchange in the western Arctic coastal ocean. *Global Biogeochemical Cycles*, (October), n/a–n/a. http://doi.org/10.1002/2015GB005153
21. Forest, a., Coupel, P., Else, B., Nahavandian, S., Lansard, B., Raimbault, P., … Babin, M. (2014). Synoptic evaluation of carbon cycling in the Beaufort Sea during summer: Contrasting river inputs, ecosystem metabolism and air-sea CO2 fluxes. *Biogeosciences*, *11*(10), 2827–2856. http://doi.org/10.5194/bg-11-2827-2014
22. Fujiwara, a., Hirawake, T., Suzuki, K., Imai, I., & Saitoh, S. I. (2014). Timing of sea ice retreat can alter phytoplankton community structure in the western

Arctic Ocean. *Biogeosciences*, *11*(7), 1705–1716. http://doi.org/10.5194/bg-11-1705-2014

23. Gao, Z., Chen, L., Sun, H., Chen, B., & Cai, W. J. (2012). Distributions and air-sea fluxes of carbon dioxide in the Western Arctic Ocean. *Deep-Sea Research Part II: Topical Studies in Oceanography*, *81-84*, 46–52. http://doi.org/10.1016/j.dsr2.2012.08.021
24. Giles, K. a., Laxon, S. W., Ridout, A. L., Wingham, D. J., & Bacon, S. (2012). Western Arctic Ocean freshwater storage increased by wind-driven spin-up of the Beaufort Gyre. *Nature Geoscience*, *5*(3), 194–197. http://doi.org/10.1038/ngeo1379
25. Hauri, C., Winsor, P., Juranek, L. W., McDonnell, A. M. P., Takahashi, T., & Mathis, J. T. (2013). Wind-driven mixing causes a reduction in the strength of the continental shelf carbon pump in the Chukchi Sea. *Geophysical Research Letters*, *40*(22), 5932–5936. http://doi.org/10.1002/2013GL058267
26. Hill, V., & Cota, G. (2005). Spatial patterns of primary production on the shelf, slope and basin of the Western Arctic in 2002. *Deep Sea Research Part II: Topical Studies in Oceanography*, *52*(24-26), 3344–3354. http://doi.org/10.1016/j.dsr2.2005.10.001
27. Ho, D. T., Law, C. S., Smith, M. J., Schlosser, P., Harvey, M., & Hill, P. (2006). Measurements of air-sea gas exchange at high wind speeds in the Southern Ocean: Implications for global parameterizations. *Geophysical Research Letters*, *33*(16).
28. Holm-Hansen, O., Lorenzen, C. J., Holmes, R. W., & Strickland, J. D. (1965). Fluorometric determination of chlorophyll. *Journal du Conseil*, *30*(1), 3-15.
29. Jeffries, M. O., Richter-Menge, J., Overland, J.E. Eds., (2014): Arctic Report Card 2014, http://www.arctic.noaa.gov/reportcard
30. Jiang, L.-Q., Cai, W.-J., Wanninkhof, R., Wang, Y., & Lüger, H. (2008). Air-sea CO2 fluxes on the U.S. South Atlantic Bight: Spatial and seasonal

variability. *Journal of Geophysical Research*, *113*(C7), 1–17. http://doi.org/10.1029/2007JC004366

31. Jones, E. P., Anderson, L. G., Jutterström, S., Mintrop, L., & Swift, J. H. (2008). Pacific freshwater, river water and sea ice meltwater across Arctic Ocean basins: Results from the 2005 Beringia Expedition. *Journal of Geophysical Research*, *113*(C8), C08012. http://doi.org/10.1029/2007JC004124
32. Lepore, K., Moran, S. B., Grebmeier, J. M., Cooper, L. W., Lalande, C., Maslowski, W., … Kelly, R. P. (2007). Seasonal and interannual changes in particulate organic carbon export and deposition in the Chukchi Sea. *Journal of Geophysical Research*, *112*(C10), 1–14. http://doi.org/10.1029/2006JC003555
33. Loose, B., Miller, L., Elliot, S., & Papakyriakou, T. (2011). Sea Ice Biogeochemistry and Material Transport Across the Frozen Interface. *Oceanography*, *24*(3), 202–218. http://doi.org/10.5670/oceanog.2011.72
34. Lowry, K. E., van Dijken, G. L., & Arrigo, K. R. (2014). Evidence of under-ice phytoplankton blooms in the Chukchi Sea from 1998 to 2012. *Deep Sea Research Part II: Topical Studies in Oceanography*, *105*, 105–117. http://doi.org/10.1016/j.dsr2.2014.03.013
35. Martin, J., Tremblay, J. Eric, Gagnon, J., Tremblay, G., Lapoussire, A., Jose, C., Michel, C. (2010). Prevalence, structure and properties of subsurface chlorophyll maxima in Canadian Arctic waters. *Marine Ecology Progress Series*, *412*(May), 69–84. http://doi.org/10.3354/meps08666
36. Nishino, S., Kikuchi, T., Yamamoto-Kawai, M., Kawaguchi, Y., Hirawake, T., & Itoh, M. (2011). Enhancement/reduction of biological pump depends on ocean circulation in the sea-ice reduction regions of the Arctic Ocean. *Journal of Oceanography*, *67*(3), 305–314. http://doi.org/10.1007/s10872-011-0030-7
37. Nishino, S., Kawaguchi, Y., Inoue, J., Hirawake, T., Fujiwara, A., Futsuki, R., Aoyama, M. (2015). Nutrient supply and biological response to wind-induced

mixing, inertial motion, internal waves, and currents in the northern Chukchi Sea. *Journal of Geophysical Research : Oceans*, *120*(May), 1975–1992. http://doi.org/10.1002/2014JC010407.Received

38. Overpeck, J. T., Sturm, M., Francis, J. a., Perovich, D. K., Serreze, M. C., Benner, R., Vörösmarty, C. (2005). Arctic system on trajectory to new, seasonally ice-free state. *Eos, Transactions American Geophysical Union*, *86*(34), 309. http://doi.org/10.1029/2005EO340001
39. Pabi, S., van Dijken, G. L., & Arrigo, K. R. (2008). Primary production in the Arctic Ocean, 1998-2006. *Journal of Geophysical Research: Oceans*, *113*(8), 1998–2006. http://doi.org/10.1029/2007JC004578
40. Papadimitriou, S., Kennedy, H., Kattner, G., Dieckmann, G. S., & Thomas, D. N. (2004). Experimental evidence for carbonate precipitation and CO2 degassing during sea ice formation. *Geochimica et Cosmochimica Acta*, *68*(8), 1749–1761. http://doi.org/10.1016/j.gca.2003.07.004
41. Perovich, D. K. Light, B., Eicken, H., Jones, K. F., Runciman, K., and Nghiem, S. V. (2007) Increasing solar heating of the Arc- tic Ocean and adjacent seas, 1979–2005: Attribution and role in the ice-albedo feedback, Geophys. Res. Lett., 34, L19505, doi:10.1029/2007GL031480, 2007
42. Perrette, M., Yool, A., Quartly, G. D., & Popova, E. E. (2011). Near-ubiquity of ice-edge blooms in the Arctic. *Biogeosciences*, *8*(2), 515–524. http://doi.org/10.5194/bg-8-515-2011
43. Peterson, B. J., Holmes, R. M., McClelland, J. W., Vörösmarty, C. J., Lammers, R. B., Shiklomanov, A. I., … Rahmstorf, S. (2002). Increasing river discharge to the Arctic Ocean. *Science (New York, N.Y.)*, *298*(5601), 2171–2173. http://doi.org/10.1126/science.1077445
44. Pipko, I. I., Semiletov, I. P., Tishchenko, P. Y., Pugach, S. P., & Christensen, J. P. (2002). Carbonate chemistry dynamics in Bering Strait and the Chukchi Sea. *Progress in Oceanography*, *55*(1-2 SPEC ISS.), 77–94. http://doi.org/10.1016/S0079-6611(02)00071-X

45. Rysgaard, S., Glud, R. N., Sejr, M. K., Bendtsen, J., & Christensen, P. B. (2007). Inorganic carbon transport during sea ice growth and decay: A carbon pump in polar seas. *Journal of Geophysical Research: Oceans*, *112*(3), 1–8. http://doi.org/10.1029/2006JC003572
46. Rysgaard, S., Bendtsen, J., Delille, B., Dieckmann, G. S., Glud, R. N., Kennedy, H., Tison, J. L. (2011). Sea ice contribution to the air-sea CO2 exchange in the Arctic and Southern Oceans. *Tellus, Series B: Chemical and Physical Meteorology*, *63*(5), 823–830. http://doi.org/10.1111/j.1600-0889.2011.00571.x
47. Schröder, D., Feltham, D. L., Flocco, D., & Tsamados, M. (2014). September Arctic sea-ice minimum predicted by spring melt-pond fraction. *Nature Climate Change*, *4*(5), 353–357. http://doi.org/10.1038/NCLIMATE2203
48. Semiletov, I. P., Pipko, I. I., Repina, I., & Shakhova, N. E. (2007). Carbonate chemistry dynamics and carbon dioxide fluxes across the atmosphere-ice-water interfaces in the Arctic Ocean: Pacific sector of the Arctic. *Journal of Marine Systems*, *66*(1-4), 204–226. http://doi.org/10.1016/j.jmarsys.2006.05.012
49. Serreze, M. C., Maslanik, J. A., Scambos, T. A., Fetterer, F., Stroeve, J., Knowles, K., … Haran, T. M. (2003). A record minimum arctic sea ice extent and area in 2002. *Geophysical Research Letters*, *30*(3), 1–4. http://doi.org/10.1029/2002GL016406
50. Springer, A. M., & McRoy, C. P. (1993). The paradox of pelagic food webs in the northern Bering Sea—III. Patterns of primary production. *Continental Shelf Research*, *13*(5-6), 575-599.
51. Stroeve, J., Holland, M. M., Meier, W., Scambos, T., and Serreze, M. (2007) Arctic sea ice decline: Faster than forecast, Geophys. Res. Lett., 34(9), L09501, doi:10.1029/2007GL029703
52. Tanhua, T., Jones, E. P., Jeansson, E., Jutterström, S., Smethie, W. M., Wallace, D. W. R., & Anderson, L. G. (2009). Ventilation of the arctic ocean: Mean ages and inventories of anthropogenic CO2 and CFC-11. *Journal of*

Geophysical Research: Oceans, *114*(1), 1–11. http://doi.org/10.1029/2008JC004868

53. Wanninkhof, R. (1992). Relationship Between Wind Speed and Gas Exchange. *Journal of Geophysical Research*, *97*(92), 7373–7382. http://doi.org/10.1029/92JC00188
54. Welschmeyer Nicholas A. , (1994), Fluorometric analysis of chlorophyll a in the presence of chlorophyll b and pheopigments, Limnology and Oceanography, 39, doi: 10.4319/lo.1994.39.8.1985.
55. Woodgate, R. a., Weingartner, T. J., & Lindsay, R. (2012). Observed increases in Bering Strait oceanic fluxes from the Pacific to the Arctic from 2001 to 2011 and their impacts on the Arctic Ocean water column. *Geophysical Research Letters*, *39*, 2–7. http://doi.org/10.1029/2012GL054092
56. Yang, J. (2009). Seasonal and interannual variability of downwelling in the Beaufort Sea. *Journal of Geophysical Research*, *114*(August 2008), C00A14. http://doi.org/10.1029/2008JC005084
57. Yamamoto-Kawai, M., McLaughlin, F. a., Carmack, E. C., Nishino, S., & Shimada, K. (2008). Freshwater budget of the Canada Basin, Arctic Ocean, from salinity, δ18O, and nutrients. *Journal of Geophysical Research: Oceans*, *113*(1), 1–12. http://doi.org/10.1029/2006JC003858
58. Yamamoto-Kawai, M., McLaughlin, F. a., Carmack, E. C., Nishino, S., Shimada, K., & Kurita, N. (2009). Surface freshening of the Canada Basin, 2003-2007: River runoff versus sea ice meltwater. *Journal of Geophysical Research: Oceans*, *114*(4), 2003–2007. http://doi.org/10.1029/2008JC005000
59. Zhang, J., Ashjian, C., Campbell, R., Spitz, Y. H., Steele, M., & Hill, V. (2015). The influence of sea ice and snow cover and nutrient availability on the formation of massive under-ice phytoplankton blooms in the Chukchi Sea. *Deep Sea Research Part II: Topical Studies in Oceanography*, *118*, 1–14. http://doi.org/10.1016/j.dsr2.2015.02.00

Appendix A

CORRESPONDENCE

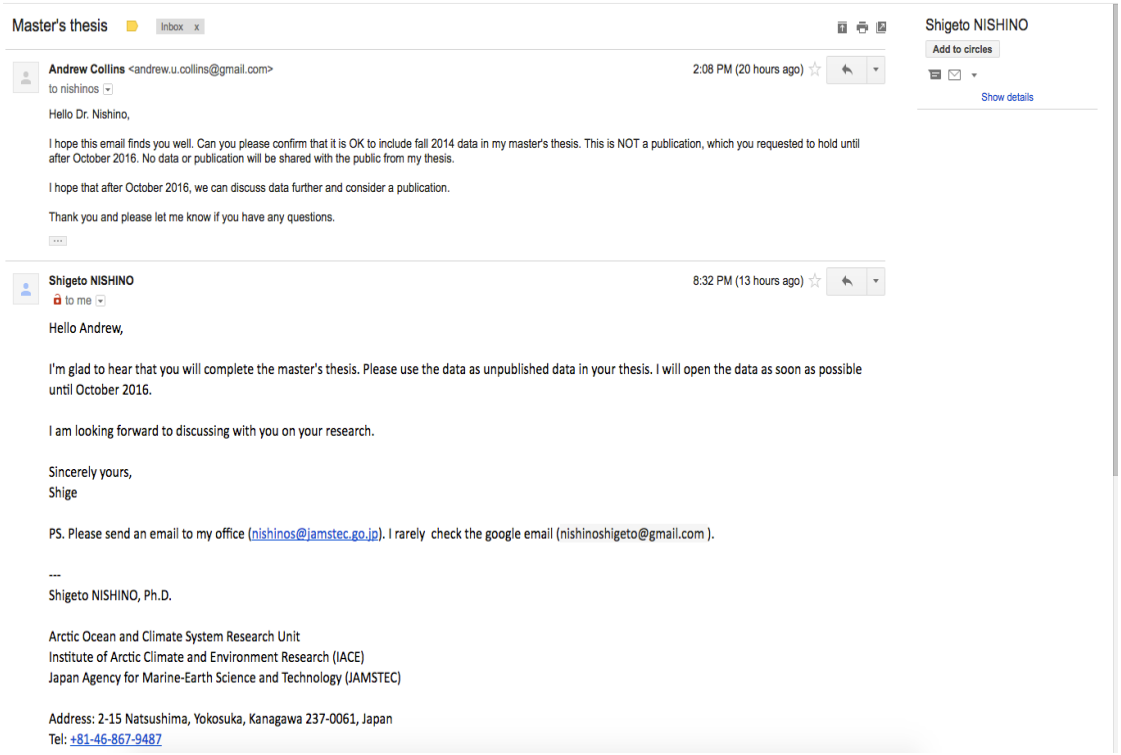

Master's thesis Inbox x

Andrew Collins <andrew.u.collins@gmail.com> 2:08 PM (20 hours ago)
to nishinos

Hello Dr. Nishino,

I hope this email finds you well. Can you please confirm that it is OK to include fall 2014 data in my master's thesis. This is NOT a publication, which you requested to hold until after October 2016. No data or publication will be shared with the public from my thesis.

I hope that after October 2016, we can discuss data further and consider a publication.

Thank you and please let me know if you have any questions.

Shigeto NISHINO 8:32 PM (13 hours ago)
to me

Hello Andrew,

I'm glad to hear that you will complete the master's thesis. Please use the data as unpublished data in your thesis. I will open the data as soon as possible until October 2016.

I am looking forward to discussing with you on your research.

Sincerely yours,
Shige

PS. Please send an email to my office (nishinos@jamstec.go.jp). I rarely check the google email (nishinoshigeto@gmail.com).

Shigeto NISHINO, Ph.D.

Arctic Ocean and Climate System Research Unit
Institute of Arctic Climate and Environment Research (IACE)
Japan Agency for Marine-Earth Science and Technology (JAMSTEC)

Address: 2-15 Natsushima, Yokosuka, Kanagawa 237-0061, Japan
Tel: +81-46-867-9487

Shigeto NISHINO
Add to circles
Show details

Letter granting permission for use of auxilliary data.